Research in Astron. Astrophys. **2010** Vol. **10** No. **10**, 956–1004
http://www.raa-journal.org *http://www.iop.org/journals/raa*

Research in Astronomy and Astrophysics

INVITED REVIEWS

Optical gravitational wave detectors on the ground and in space: theory and technology

Jean-Yves Vinet

ARTEMIS Observatoire de la Côte d'Azur Université de Nice-Sophia Antipolis 06304 NICE, France; *vinet@oca.eu*

Received 2010 February 14; accepted 2010 April 26

Abstract Major predictions of General Relativity, unforeseen at the beginning of the preceding century, are now under investigation. The existence of black holes of any mass from tens to billions of solar masses is now established, and the physics around these objects begins to be studied through direct observations in a wide electromagnetic spectrum from visible light to X-rays. General relativity, however, provides an extra medium which carries more information on the regions of intense gravitational field, namely gravitational waves (GWs). Due to their extremely weak coupling to matter, GWs are precisely generated in those regions of spacetime undergoing strong curvature, which is very exciting for modern astrophysics. On the other hand, this weak coupling makes it difficult for GWs to cause appreciable effects in human made instruments. This is why technology of GW detectors took such a long time to reach a sensitivity level consistent with GW amplitudes predicted by theoretical models of sources. In the present status, apart from resonant solid detectors, two large interferometric antennas (LIGO in the USA and the French-Italian Virgo) are beginning to produce data, and a joint ESA-NASA space mission, resulting from a wide effort of European and American groups, is reaching a crucial approval phase. The aim of the present review is to give the theoretical bases of GW detectors using light.

Key words: gravitation — gravitational waves — interferometry

1 BIRTH OF GRAVITATIONAL WAVE ASTRONOMY

Direct detection of gravitational waves by physics instruments is an old dream that began in the sixties after the pioneering experiments of Weber (1960). These experiments soon proved negative, and realistic estimates of the gravitational wave amplitudes on Earth showed that they were far below the sensitivity threshold of Weber's antenna. The momentum was nevertheless started and a number of teams undertook developing more sensitive instruments. Forty years later, it appears that these first experiments have given birth to a new field of research in which several areas of expertise come into close contact, and of which intrinsic interest would be seriously weakened without all others. These areas of expertise are the theory of gravitation, relativistic astrophysics, numerical relativity, signal processing, and metrology, which all combine in the field of Gravitational Wave Astronomy (GWA). Two important phases in the fifty year old history of GWA are the first real concept for a large scale Michelson laser interferometer by Weiss (1972) at MIT, then the introduction of resonant cavities into this scheme by Drever (1983) at Glasgow, then at Caltech. This was the seed of the

LIGO project, and further of the Virgo project, led by Alain Brillet and Adalberto Giazotto. After a brief recall of gravitational wave emission and the first experiments based on resonant solids, this review essentially addresses the concept of a ground detector based on the Michelson topology and on properties of resonant (Fabry-Perot) cavities. During the same four decades, the concept of a space interferometer was devised and discussed by Peter Bender at JILA and later by Ronald Hellings at NASA. The second part of this review discusses some of the main features of the space mission LISA which is the outcome of this long development.

2 EMISSION OF GRAVITATIONAL WAVES

2.1 Theory

Gravitational waves (GW) are a consequence of Einstein's General Relativity (GR) in the same way as electromagnetic waves come from Maxwell's Electrodynamics. In the framework of Special Relativity, in a system of coordinates x^λ, an electromagnetic wave is described (in vacuum) by the vector field $A_\mu(x^\lambda)$ (4-potential) obeying the Maxwell equations. The wave, which propagates at velocity c, is transverse and has two polarization components. In GR, the gravitational state of spacetime is associated with its geometry through the metric tensor $g_{\mu\nu}(x^\lambda)$ obeying the Einstein equations. In the case of a gravitational wave far from its source, in a freely falling reference system, one can write

$$g_{\mu\nu}(t,\boldsymbol{x}) = \eta_{\mu\nu} + h_{\mu\nu}(t,\boldsymbol{x}), \tag{1}$$

where $\eta_{\mu\nu} \equiv \mathrm{diag}(1,-1,-1,-1)$ is the Minkowski tensor of the locally flat background spacetime (freely falling frame), and $h_{\mu\nu}$ is a very small dimensionless tensor field representing the GW amplitude. It can be shown that $h_{\mu\nu}$ can eventually be reduced to only two independent functions $h_+, h_\times$ defining the polarization state of the wave. Gravitational waves are emitted by distributions of matter/energy having a time dependent quadrupole moment. In the transverse-traceless gauge, at the first level of the approximation, only the space components are significant and have an expression analogous to a retarded potential (Tourrenc 1997)

$$h_{jk}(t,r) = \frac{2G}{c^4}\frac{1}{r}\,\partial_t^2\,\left[\Xi_{jk}(t-r/c)\right]^{\mathrm{TT}}, \qquad (r \equiv \boldsymbol{x}^2) \tag{2}$$

where the symbol TT refers to the projection on the transverse plane of the symmetric traceless quadrupole tensor $\Xi(t)$ defined by the volume integral

$$\Xi_{jk}(t) = \int \rho(t,\boldsymbol{x})\left[x^i x^j - \frac{1}{3}\,\delta_{jk}\,\boldsymbol{x}^2\right] d^3x,$$

where ρ is the density of matter. Further levels of approximation have been thoroughly investigated (Blanchet et al. 2005), but the preceding "quadrupole formula" gives an order of magnitude estimate. One immediately notes the extreme weakness of the coupling coefficient G/c^4 which is the cause of all technological challenges encountered on the way to GW astronomy. Only astrophysical events involving stars or black holes in a nearly relativistic velocity regime can cause amplitudes of GWs larger than 10^{-23} in the neighborhood of the Earth. If we denote by h the maximum value of the $h_{\mu,\nu}$ tensor, existing instruments have been designed for a sensitivity of about $h \sim 10^{-22\pm1}$ in the middle of the bandwidth, (around 500 Hz for terrestrial instruments, 1 mHz for space antennas) which seemed to be the most feasible at the time when the preliminary R&D studies ended.

2.2 GW Signals

The sources of gravitational waves may be classified according to their frequency domain. Roughly speaking, high frequency waves are emitted by systems of light bodies whereas very massive systems radiate at low frequency. There is no lower bound, because in principle any couple of objects

orbiting each other radiate at some level (even the Earth around the Sun). There is a generally admitted upper bound fixed by the final frequency of the coalescence of a neutron star binary, each with 1.4 solar masses, namely at a few kHz. From a technological point of view, the low frequency range is addressed by the bandwidth of LISA: [0.1 mHz, 0.1 Hz], and the high frequency range by the bandwidth of Virgo/LIGO: [10 Hz, 10 kHz]. There is thus a gap in the possible frequencies which is a target for a possible future space Japanese project named "DECIGO."[1]These ranges are in turn determined by strong constraints. The lower bound of 10 Hz for terrestrial instruments results from the level of seismic motions of the ground impossible to filter out. The lower bound of 0.1 mHz for space instruments results from the performances of space accelerometers used for drag-free operation. The upper bound of 0.1 Hz for a space-based instrument like LISA results from the Signal to Noise Ratio (SNR) which involves the quantum noise level and the transfer function of the instrument for gravitational wave signals. The transfer function could be changed for a different size of the instrument. The bounds could be somewhat modified but not dramatically changed. Thus for those technological reasons, there are two kinds of sources addressed by the two complementary kinds of instruments.

2.2.1 High frequency sources

The first type of source foreseen in the seventies, at the time of the Weber experiments, was the supernova events, or more precisely, the collapse of a giant star to a neutron star or to a stellar black hole. Estimations of the amplitude of gravitational waves on the ground caused by such events have been intensively performed by numerical simulations (Bonazzola & Marck 1993; Zwerger & Mueller 1997). A perfectly radial collapse would generate no quadrupolar moment, and therefore no gravitational wave. However, some degree of asymmetry may be imagined. For instance, according to Thorne (1987), if we denote by ϱ the fraction of the mass of the star converted in gravitational radiative energy, by f_c a characteristic frequency (a time average of the frequency during the pulse, weighted by the instantaneous power of the pulse) and by r the distance to the source, we would have an average amplitude during the pulse

$$h = 2.7 \times 10^{-20}\, \varrho^{1/2} \left[\frac{1\mathrm{kHz}}{f_c}\right]^{1/2} \left[\frac{10\,\mathrm{Mpc}}{r}\right].$$

Estimations of ϱ have been continuously decreasing, reaching around $\sim 10^{-5}$. The characteristic frequency is on the order of ~ 500 Hz. These figures must be taken as guidelines rather than firm predictions. The details of the internal dynamics of collapses are still poorly understood. The second type of source is a rotating neutron star having some degree of asymmetry resulting in a quadrupole moment. Several mechanisms have been invoked for creating such an asymmetry, regarding the internal motion of the neutron fluid. Examples are the Chandrasekhar-Friedmann-Schutz (Chandrasekhar 1970) instability, or the transition from a neutron star to a quark star. Here also, the estimations of the quadrupole are rather fuzzy. The third type, which is more promising, is the inspiral and coalescence of two compact objects like neutron stars or stellar black holes. Compacts objects can have short orbits and consequently high velocities. Their gravitational emission is thus significant and so is their energy loss per orbit. This has been directly observed for the double pulsar 1913+16. The energy loss results in a decrease of the size of the orbit and an increase of the velocity and consequently of the gravitational wave emission. This positive feedback ends by the final inspiral and merging of the two bodies to form a final unique black hole. This scenario has been extensively studied by analytical methods (post-Newtonian expansions) or numerically. An estimation of the gravitational

[1] *http://tamago.mtk.nao.ac.jp/spacetime/decigo_e.html*

characteristic amplitude is, still following Thorne (1987):

$$h_c = 4 \times 10^{-22} \left[\frac{\mu}{M_\odot}\right]^{1/2} \left[\frac{M}{M_\odot}\right]^{1/2} \left[\frac{100\,\mathrm{Mpc}}{r}\right] \left[\frac{100\,\mathrm{Hz}}{f_c}\right],$$

where the characteristic frequency is typically 1.44 times the lower bound of the detector, μ is the reduced mass of the system and M is the total mass (i.e. $M \equiv m_1 + m_2$ and $\mu \equiv m_1 m_2/M$). $M_\odot$ refers to the mass of the Sun.

2.2.2 Low frequency sources

In the low frequency domain, we find three types of emissions.

The first type refers to the whole population of galactic white dwarfs having orbital periods of a few hours or less. These are purely monochromatic sources, with amplitudes given by a simple model (Tourrenc 1997), at least in the case of two equal masses M with a circular orbit of radius $R/2$:

$$h_+ = \frac{4G^2M^2}{c^4rR}\,\frac{1+\cos^2 i}{2}\cos(2\Phi),$$

$$h_\times = \frac{4G^2M^2}{c^4rR}\,\cos i\,\sin(2\Phi),$$

where $\Phi \equiv 2\pi t/[T = 1\,\mathrm{yr}]$ is the orbital phase, and i the inclination of the angular momentum with respect to the line of sight.

The second type is the capture of compact bodies by a massive or supermassive black hole (Hughes 2001) after a more or less complex orbital sequence (EMRI = Extreme Mass Ratio Inspiral). Such events could have occurrence frequencies such that several of them could be detected per year by LISA (Gair & Jones 2006).

The third type of low frequency source is again the inspiral of comparable mass binaries. In the case of supermassive black holes, the relativistic regime is such that effects like spin-orbit or spin-spin couplings could be significant in the signal's details. A simple example, based on the Effective One Body approach (Buonanno & Damour 2000) (neglecting spin effects) is shown in Figure 1.

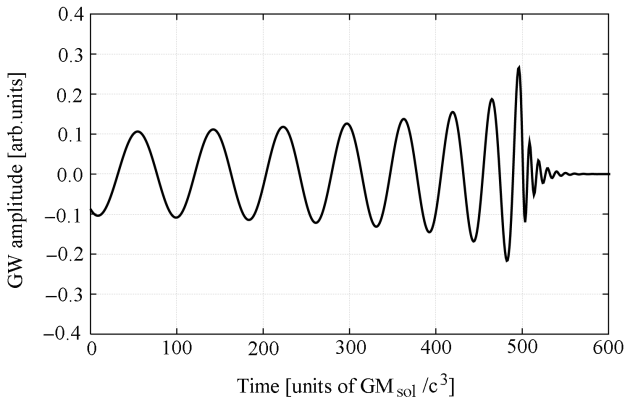

Fig. 1 Generic waveform generated by a binary inspiral followed by the merging of the two neutron stars (or black holes), and the final ringdown of the resulting black hole.

One can see the inspiral part, the merger phase of the two black holes and the ringdown of the final black hole.

3 SOME PHYSICS IN A WAVY SPACETIME

Being a perturbation of the geometry of spacetime, one can expect GWs to produce some distortions in high precision metrology experiments. We briefly recall the existence of narrow band solid antennas, then focus on optical experiments.

3.1 Continuous Media

The first experiment, which was proposed by Weber (Weber 1960), rested on the idea that a GW could induce stresses in solids (tidal effects), and that on a suitably isolated solid resonator, weakly dissipative in terms of acoustic waves, one could detect with some transducer system, the resonances occurring when the GW signal overlaps its acoustical bandwidth. This idea is supported by a general relativistic extension of the linear elasticity theory (Vinet 1979). The result is the modified tensor elastodynamic equation

$$\rho\ddot{E}_{ij} - \frac{1}{2}\left[\partial_k\partial_j\Theta_{ik} + \partial_k\partial_i\Theta_{jk}\right] = -\frac{1}{2}\,\rho\,\ddot{h}_{ij}, \tag{3}$$

where E_{ij} (resp. Θ_{ij}) is the classical strain (resp. stress) tensor, and ρ the density. If we take the origin of coordinates at the center of mass, and if we assume a GW wavelength much larger than the size of the resonator, this can be regarded as the derivative of the following generalized Navier-Cauchy equation:

$$\rho\ddot{u}^i - \partial_k\Theta^{ik} = -\frac{1}{2}\,\rho\,\ddot{h}^{ij}x^j, \tag{4}$$

where $\boldsymbol{u}$ is the displacement vector. The GW amplitude thus appears as a driving internal force, of tidal type, acting on the resonator. After the controversial but negative results of Weber, several groups nevertheless built hugely improved versions of the Weber antenna. These instruments, called "bar antennas," have been built in several countries (for a generic example of such an antenna, see Fig. 2). The most well-known are ALLEGRO (Louisiana State University, USA, Mauceli et al. 1996), AURIGA (Legnaro, Istituto di Fisica Nucleare, Italy, Baggio et al. 2005), NAUTILUS, (Frascati, INFN, Italy, Astone et al. 2006), EXPLORER (Rome University, at CERN, Astone et al. 1993, 2008), and NIOBE (University of Western Australia[2]). Large resonators like GRAIL with spherical shapes have been planned (Gottardi 2007) after the development of a small size spherical resonator MINIGRAIL (de Waard et al. 2005). Because the Brownian thermal noise is the main limitation to their sensitivity, a common feature of these experiments is their operation at very low temperature (a few mK), which implies complex circulations of cryogenic fluids.

As with any resonator, bars have a very short bandwidth (up to a few tens of Hz), so that reconstructing a waveform after a GW event has been detected is problematic (note that a larger bandwidth could, however, be achieved in a detector like GRAIL). This explains why "bar physicists" progressively transfer their expertise to interferometers. This is also why we focus on optical experiments from now on, which are intrinsically wideband.

3.2 Gravitational Waves and Light

A more direct physical effect of GWs is to modulate the light distances between freely falling test masses. In a vacuum, light is expected to propagate along a null geodesic, which means that the invariant element of spacetime $ds^2 \equiv g_{\mu\nu}dx^\mu dx^\nu$ is identically zero along any optical path. With

[2] *http://www.gravity.uwa.edu.au/Stageone.html*

Fig. 2 Generic structure of a resonant solid GW antenna: Example of the antenna "AURIGA" (Legnaro, Italy).

the expression (1) of the metric tensor, one can suspect that the effective optical paths of photons will be perturbed.

3.2.1 Arbitrary wavelength

In the case of very long range optical paths (e.g. 5 Mkm in the case of LISA), one must take into account the action of the GW during light propagation. If a light beam of fixed frequency is emitted from spacecraft A and detected at spacecraft B, the nominal distance AB being L and $\boldsymbol{n}$ being the unit vector from A to B, the physical effect detected at B is a frequency modulation. Let $\boldsymbol{w}$ be a unit vector along the propagation direction of the GW, and let us define two more unit vectors, mutually orthogonal in the transverse plane

$$\boldsymbol{\vartheta} = \frac{\partial \boldsymbol{w}}{\partial \theta}, \qquad \boldsymbol{\varphi} = \frac{1}{\sin\theta}\,\frac{\partial \boldsymbol{w}}{\partial \phi},$$

then the two directional functions

$$\xi_+(\theta,\phi) = (\boldsymbol{\vartheta}\cdot\boldsymbol{n})^2 - (\boldsymbol{\varphi}\cdot\boldsymbol{n})^2, \qquad \xi_\times(\theta,\phi) = 2(\boldsymbol{\vartheta}\cdot\boldsymbol{n})(\boldsymbol{\varphi}\cdot\boldsymbol{n}),$$

are incorporated in the function

$$H(t) = h_+(t)\,\xi_+(\theta,\phi) \;+\; h_\times(t)\,\xi_\times(\theta,\phi)\,. \tag{5}$$

Now the observable effect is a relative frequency modulation, analogous to a Doppler shift (Dhurandhar et al. 2002), given by ($c = 1$)

$$\left[\frac{\delta\nu(t)}{\nu}\right]_{A\to B} = \frac{H(t - \boldsymbol{w}\cdot\boldsymbol{x}_B) - H(t - \boldsymbol{w}\cdot\boldsymbol{x}_A - L)}{2(1 - \boldsymbol{w}\cdot\boldsymbol{n})}, \tag{6}$$

where $\boldsymbol{x}_A$ and $\boldsymbol{x}_B$ are the positions of the two spacecraft. This is often called a "two pulses" response, because a short GW pulse would be recorded twice by a phasemeter at B.

3.2.2 Long wavelength limit

The expected frequencies of GW events, for obvious reasons, are much lower (at most a few kHz) than optical frequencies. In this regime, the only effect of a GW on light is to perturb the flight time of photons between two test masses (light distances). Consider a light path lying in the (x, y) plane, either along the x (north) or the y (west) axis. Consider on the other hand a GW propagating along a direction of unit vector $\boldsymbol{w}$.

$$\boldsymbol{w} = \begin{pmatrix} \sin\theta\cos\phi \\ \sin\theta\sin\phi \\ \cos\theta \end{pmatrix}. \tag{7}$$

If $h_+, h_\times$ are the two polarization components of the wave, the effect of the GW is to create a phase modulation on the two beams

$$\Phi_{\rm north}(t) = \frac{2\pi L}{\lambda}\left[h_+(t)(\cos^2\theta\cos^2\phi - \sin^2\phi) - h_\times(t)\cos\theta\sin 2\phi\right], \tag{8}$$

$$\Phi_{\rm west}(t) = \frac{2\pi L}{\lambda}\left[h_+(t)(\cos^2\theta\sin^2\phi - \cos^2\phi) + h_\times(t)\cos\theta\sin 2\phi\right]. \tag{9}$$

In an interferometric configuration, where the observable is a differential phase, this gives:

$$\Delta\Phi(t) = \frac{4\pi L}{\lambda}\left[h_+(t)\,\frac{1+\cos^2\theta}{2}\,\cos 2\phi - h_\times(t)\cos\theta\sin 2\phi\right], \tag{10}$$

where it can be seen that the interferometer acts like a transducer, converting the gravitational signal into a phase and eventually into an electrical signal through some photo detector.

4 LONG BASELINE TERRESTRIAL ANTENNAS

The general features of a ground based GW interferometric antenna are summarized by Figure 3. The main part comprises two long cavities (3 km for Virgo, 4 km for the LIGO's). The role of the resonant cavities is to extend the physical length of a few km to an effective one of a few hundreds of km. The role of the recycling mirror is to build an embedding resonant cavity with the Michelson interferometer considered as a virtual reflector when tuned at a dark fringe. In this section, we explain and discuss these items.

4.1 General Principles of Interferometry

4.1.1 Basic Michelson interferometer

We first consider a basic Michelson interferometer involving only two mirrors and one splitter (see Fig. 4).

The light source of wavelength λ is modeled by a complex amplitude A. The outgoing amplitude B is

$$B = r_s t_s A\left(r_1 \mathrm{e}^{2ika} + r_2 \mathrm{e}^{2ikb}\right),$$

where r_s and t_s are the amplitude reflection and transmission coefficients of the splitter (hopefully both near $1/\sqrt{2}$) respectively, and r_1, r_2 the amplitude reflection coefficients of the end mirrors (hopefully near 1). We have set $k \equiv 2\pi/\lambda$. If we interpret $|A|^2$ and $|B|^2$ as respectively the incoming

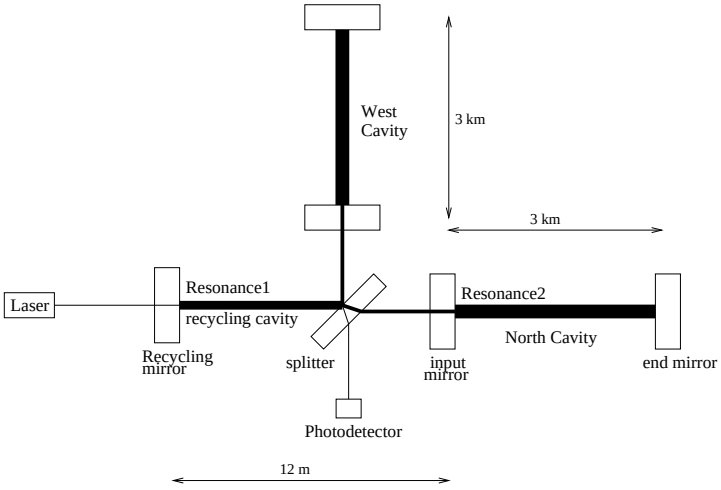

Fig. 3 Simplified layout of the Virgo antenna.

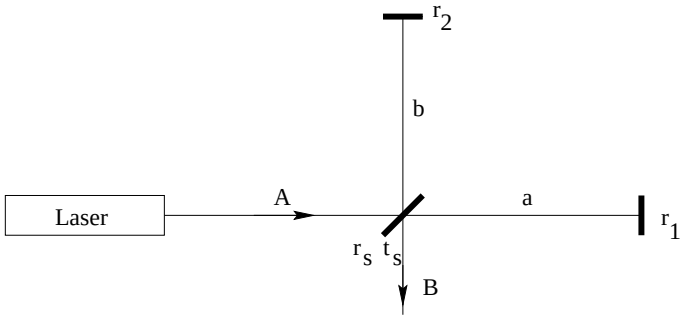

Fig. 4 A basic Michelson interferometer.

and outgoing intensities, or up to a constant, the area S of the detector as the incoming and outgoing powers, a photodetector receiving wave B will record the power

$$P_B = P_{\mathrm{L}} r_s^2 t_s^2 \left[r_1^2 + r_2^2 + 2 r_1 r_2 \cos\left(2k(b-a)\right) \right], \tag{11}$$

where P_{L} is the laser power on the effective area S. By tuning the optical path difference $b-a$, one can obtain constructive interference ($2k(b-a) \equiv 2\pi$)

$$P_{B,\max} = P_{\mathrm{L}} r_s^2 t_s^2 (r_1 + r_2)^2,$$

if both r_s and t_s are near $1/\sqrt{2}$ and if r_1, r_2 are near unity, we see that the outgoing power is near the incoming one, and the tuning corresponds to the so called bright fringe. We obtain destructive interference with ($2k(b-a) \equiv \pi$)

$$P_{B,\min} = P_{\mathrm{L}} r_s^2 t_s^2 (r_1 - r_2)^2,$$

which can be made extremely small with mirrors as similar as possible, knowing that perfectly identical mirrors are beyond the possibilities of present technology. The ratio

$$P_{B,\max}/P_{B,\min} = \left(\frac{r_1 + r_2}{r_1 - r_2}\right)^2$$

is called contrast.

4.1.2 Continuous detection

Such a device may be used to detect small motions of one of the two mirrors. Assume for instance a time variation of length a

$$a = a_0 + x(t).$$

The interferometric setup was necessary since $x \ll \lambda$. We can linearize (11) and write

$$P_B = P_{\mathrm{DC}} + P_x(t),$$

where

$$P_{\mathrm{DC}} = P_{\mathrm{L}}\, r_s^2 t_s^2 \left(r_1^2 + r_2^2 + 2r_1 r_2 \cos\phi\right),$$

$\phi \equiv 2k(b - a_0)$ is the static tuning of the interferometer, and

$$P_x(t) = 4P_{\mathrm{L}}\, r_s^2 t_s^2 r_1 r_2\, \sin\phi\, kx(t).$$

The outgoing power thus has a component proportional to the motion to be detected. The first fundamental limit in the detection process comes from the fact that even in the absence of motion ($x = 0$), the detector will nevertheless deliver a fluctuating power due to the quantum nature of the detection process. It can be shown that the power fluctuations ("quantum noise" or "shot noise") are characterized, at low frequencies compared with the bandwidth of the detector, by a (one sided) power spectral density (PSD)

$$S_{\mathrm{P}} = 2Ph_{\mathrm{P}}\nu, \tag{12}$$

where P is the constant nominal power falling on the detector, h_{P} the Planck constant and ν the light frequency. The DC component of the detected power thus has the PSD

$$S_{P_{\mathrm{DC}}} = 2P_{\mathrm{L}}h_{\mathrm{P}}\nu(r_s t_s)^2 \left(r_1^2 + r_2^2 + 2r_1 r_2 \cos\phi\right).$$

On the other hand, if we denote by S_x the PSD of x seen as a random process, we get the PSD of the signal

$$S_{P_x} = 16PL^2(r_s t_s)^4 (r_1 r_2)^2 k^2 \sin^2\phi S_x.$$

Strictly speaking, the PSD of the signal should itself involve a shot noise contribution, but we assume a motion x so small that we neglect its product with any small quantity. The random process x is therefore uncorrelated with the shot noise, so that the total PSD is simply the sum of the preceding. A signal can be detected at the output if its spectral density is larger than the shot noise PSD. We can form the signal to noise ratio (SNR) as

$$\mathrm{SNR} = \frac{S_{P_x}}{S_{P_{\mathrm{DC}}}} = \frac{8P_{\mathrm{L}}\,(r_s t_s r_1 r_2)^2 k^2 S_x\, \sin^2\phi}{h_{\mathrm{P}}\nu\,(r_1^2 + r_2^2 + 2r_1 r_2 \cos\phi)}.$$

We obviously want to optimize the SNR by choosing the best tuned ϕ. We easily find that the best tuning, giving the maximum SNR, satisfies

$$\cos\phi_{\mathrm{opt}} = -\frac{r_2}{r_1}. \tag{13}$$

(We assume $r_1 > r_2$, otherwise just permute r_1 and r_2 in the next formulas). The optimal value of SNR is now

$$\mathrm{SNR}_{\mathrm{opt}} = \frac{8P_{\mathrm{L}}}{h_{\mathrm{P}}\nu}(r_s t_s r_2)^2\, k^2\, S_x.$$

Considering $k^2 S_x$ as a small quantity, we can now make the approximation $r_s t_s r_2 \sim 1/2$, without changing the order of magnitude of the result

$$\mathrm{SNR}_{\mathrm{opt}} = \frac{2P_{\mathrm{L}}}{h_{\mathrm{P}}\nu}k^2\, S_x. \tag{14}$$

By definition, the spectral sensitivity of the device is the root PSD of the signal giving a SNR of unity

$$S_x^{1/2} = \frac{\lambda}{2\pi}\sqrt{\frac{h_{\mathrm{P}}\nu}{2P_{\mathrm{L}}}}. \tag{15}$$

If now we turn to the detection of a GW of amplitude h, we may imagine that we had a displacement $hL/2$ on one arm and $-hL/2$ on the other one, causing a total differential displacement of $x = hL$ (with $a_0 = b_0 = L$). In terms of GW amplitude, the sensitivity is therefore

$$S_h^{1/2} = \frac{\lambda}{2\pi L}\sqrt{\frac{h_{\mathrm{P}}\nu}{2P_{\mathrm{L}}}}. \tag{16}$$

We now put some figures in this simple formula. At the time when the LIGO and Virgo projects were developed, a reasonable value of laser power seemed to be a few tens of W. Let us take $P_{\mathrm{L}} = 20\,\mathrm{W}$. On the other hand, an arm length greater than a few km brings, even in desertic countries, issues related to Earth's curvature. Let us take $L = 3\,\mathrm{km}$. Going to small wavelengths, as (16) might suggest, is a bad idea, because the quality of optical components, namely the mirrors, would be rapidly spoiled, which would be a serious drawback as will be seen in the following. We assume the wavelength $\lambda \sim 1064\,\mathrm{nm}$ of an Nd: YAG laser. With these figures, we get an order of magnitude for the ultimate sensitivity of a simple Michelson

$$S_h^{1/2} \sim 4 \times 10^{-21}\ \mathrm{Hz}^{-1/2}.$$

We see that about two orders of magnitude are missing by having a detector consistent with current estimations of GW amplitudes of presently known types of sources.

4.2 Resonant Cavities

Resonant cavities have properties allowing very effective enhancements of the parameters L and P_{L} that are very important for the sensitivity. This is why we devote some discussion to a short presentation of these properties.

4.2.1 Spectral (longitudinal) properties

We first consider a Fabry-Perot cavity as a couple of mirrors having parallel surfaces and separated by a distance L (see Fig. 5).

It is now necessary to introduce a convention insuring power conservation at an interface where two waves are incoming. Consider the reflecting surface of a mirror. A wave incoming on mirror M_n, of amplitude A, is partially reflected with amplitude A_{R}, and transmitted with amplitude A_{T}. If we call respectively r_n, t_n the coefficients of the mirror (real numbers), we have firstly

$$r_n^2 + t_n^2 = 1 - p_n,$$

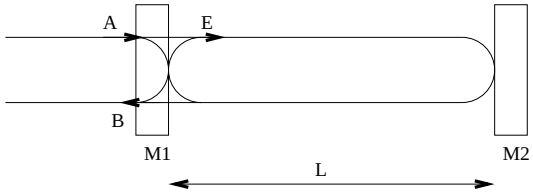

Fig. 5 Fabry-Perot interferometer.

where p_n accounts for relative power losses (absorption, diffraction by surface roughness,...). For mirrors used in advanced metrology experiments, the losses are very small, at the level of a few ppm (a few 10^{-6}). Secondly, the reflected and transmitted waves must have a $\pi/2$ phase difference. We shall take the convention

$$A_{\mathrm{R}} = ir_n A, \;\; A_{\mathrm{T}} = t_n A \;\; (i \equiv \sqrt{-1}).$$

We can now write the equation giving the intracavity amplitude E in the stationary regime

$$E = t_1 A - r_1 r_2 \mathrm{e}^{2ikL} E,$$

so that

$$S \equiv E/A = \frac{t_1}{1 + r_1 r_2 \mathrm{e}^{2ikL}}.$$

We see that S is a periodic function of the phase $\phi = 2kL$. The period in terms of frequency with the length being kept constant is

$$\Delta\nu = c/2L,$$

and is called the Free Spectral Range (FSR). The period in terms of length with the frequency being kept constant is $\Delta L = \lambda/2$, which changes the total optical path by one wavelength after reflection. Resonance obviously occurs when $\phi \equiv \pi$, giving

$$S^2_{\max} = \frac{t_1^2}{(1 - r_1 r_2)^2}. \tag{17}$$

If we consider an excursion $\delta\nu$ of the frequency with respect to a resonance ν_0, we have a corresponding phase shift of

$$\delta\phi = \frac{4\pi L \delta\nu}{c} = 2\pi \frac{\delta\nu}{\Delta\nu},$$

so that

$$|S|^2 = \frac{t_1^2}{1 + r_1^2 r_2^2 \cos 2\delta\phi} = \frac{t_1^2}{(1 - r_1 r_2)^2 + r_1 r_2 \sin^2 \delta\phi},$$

or

$$|S|^2 = S^2_{\max} \, \frac{1}{1 + \left[\frac{\sqrt{r_1 r_2}}{1 - r_1 r_2} \, \sin\left(\frac{2\pi\delta\nu}{\Delta\nu}\right)\right]^2}.$$

If further we assume a frequency excursion to be small compared to the FSR, we get

$$|S|^2 = S^2_{\max} \, \frac{1}{1 + \left[2\mathcal{F}\delta\nu/\Delta\nu\right]^2},$$

where we have used the definition of the finesse

$$\mathcal{F} \equiv \frac{\pi\sqrt{r_1 r_2}}{1 - r_1 r_2}. \tag{18}$$

It is clear that for reflectivities r_1, r_2 near unity, the finesse is a large number. The full width at half maximum of the resonance peak, or linewidth, is consequently

$$\delta\nu_{\mathrm{FWHM}} = \frac{\Delta\nu}{\mathcal{F}}.$$

One easily sees from (18) that it is possible, inversely, to express $r_1 r_2$ in terms of the finesse $\mathcal{F}$

$$r_1 r_2 = 1 - \frac{\pi}{\mathcal{F}} + \mathcal{O}(\mathcal{F}^{-2}). \tag{19}$$

We now specialize the model to a cavity used as a reflector, i.e. we assume a maximum reflectivity of M_2 and zero transmission

$$r_2^2 = 1 - p_2.$$

M_1 has some reflectivity r_1 near unity, so that

$$t_1^2 = 1 - p_1 - r_1^2,$$

and we can rewrite (17) as

$$r_2^2 S_{\max}^2 = \frac{(1 - p1)(1 - p_2) - r_1^2 r_2^2}{(1 - r_1 r_2)^2}$$

by writing $(1 - p1)(1 - p_2) \sim 1 - p_1 - p_2 = 1 - p$, where we introduce the total losses $p = p_1 + p_2$, and by substituting the approximate expression (19) found for $r_1 r_2$, we get, assuming a finesse much larger than unity

$$S_{\max}^2 \simeq \frac{2\mathcal{F}}{\pi}(1 - \sigma/2),$$

where $\sigma \equiv p\mathcal{F}/\pi$ is the so called coupling coefficient. For moderate finesse cavities, σ is still small and the last result is practically

$$S_{\max}^2 \simeq \frac{2\mathcal{F}}{\pi} \equiv N. \tag{20}$$

In the same approximation, the minimum of S is

$$S_{\min}^2 \simeq \frac{\pi}{2\mathcal{F}} = 1/N. \tag{21}$$

The reflected wave B is given by

$$B = ir_1 A + it_1 r_2 \mathrm{e}^{i\phi} E,$$

giving the reflectance of the cavity

$$R \equiv B/iA = \frac{r_1 + (1 - p_1) r_2 \mathrm{e}^{i\phi}}{1 + r_1 r_2 \mathrm{e}^{i\phi}}. \tag{22}$$

Still with the same level of approximation, we have

$$R = -\frac{1 - \sigma + 2ix}{1 - 2ix}, \tag{23}$$

where x is the reduced frequency detuning, i.e. $x \equiv (\nu - \nu_0)/\delta\nu_{\mathrm{FWHM}}$. We immediately see that the power reflectance exhibits an absorption peak at resonance

$$|R|^2 = 1 - \frac{\sigma(2-\sigma)}{1+4x^2}, \tag{24}$$

and for small σ, the defect in reflectivity, or cavity loss, is

$$p_{\mathrm{cavity}} = 2\sigma = Np. \tag{25}$$

In other words, at resonance, the global cavity losses are N times the internal losses p. For the phase reflectance we get

$$\Phi(x) = \mathrm{Arg}R = \pi + \arctan\frac{2x}{1-\sigma} + \arctan 2x. \tag{26}$$

The slope near resonance of the phase for small σ is thus

$$\left[\frac{d\Phi}{dx}\right]_{x=0} = 4.$$

For a small frequency detuning $\delta\nu$ with the cavity length being kept constant, we have

$$dx = \frac{2\mathcal{F}L}{\lambda}\,\frac{\delta\nu}{\nu_0},$$

and consequently

$$d\Phi = \frac{8\mathcal{F}L}{\lambda}\,\frac{\delta\nu}{\nu_0}.$$

For a small variation of the cavity length, with the frequency being kept constant, simply replace $L\delta\nu$ by $\nu_0\delta L$ giving

$$[d\Phi]_{\mathrm{cav}} = \frac{8\mathcal{F}L}{\lambda}\delta L.$$

If no M_1 mirror were present, the phase shift due to a single round trip would be

$$[d\Phi]_{1\ \mathrm{roundtrip}} = 2k\,\delta L = \frac{4\pi}{\lambda}\,\delta L.$$

The gain in phase shift provided by the cavity is thus

$$\frac{[d\Phi]_{\mathrm{cav}}}{[d\Phi]_{1\ \mathrm{roundtrip}}} = \frac{2\mathcal{F}}{\pi} = N.$$

The constant N precedently introduced can thus be interpreted as an effective number of round trips in the cavity.

4.3 Modal (Transverse) Properties

Practically, storage of coherent optical power in a cavity is achieved through spherical mirrors. Let us briefly recall the fundamentals. The Maxwell equations in a vacuum lead to a wave equation for the electric field, then assuming a monochromatic wave of frequency $\nu = \omega/2\pi$, for the Helmholtz equation

$$\left[\Delta + k^2\right]\mathcal{E} = 0,$$

where $k \equiv \omega/c$ and $\mathcal{E}$ is any component of the electric field. Assuming a preferred propagation direction (namely the z axis), and considering the solution as a plane wave (carrier) spatially modulated by a slowly varying envelope, we can write

$$\mathcal{E}(x,y,z) = \mathrm{e}^{ikz}\, E(x,y,z),$$

where the fast varying part of the field has been extracted in the exponential term. The remaining envelope E is such that in the second z derivative

$$\partial_z^2 \mathcal{E} = \mathrm{e}^{ikz}\left[\partial_z^2 E + 2ik\partial_z E - k^2 E\right],$$

the second order derivative can be neglected with respect to k times the first derivative. The result is the paraxial diffraction equation

$$\left[\partial_x^2 + \partial_y^2 + 2ik\partial_z\right] E(x,y,z) = 0. \tag{27}$$

It is classically shown that the equation admits families of orthogonal gaussian modes. The two most popular families are the Hermite-Gauss (HG) and the Laguerre-Gauss modes (LG). The normalized HG modes are defined by

$$\begin{aligned}\mathrm{HG}_{mn}(x,y,z) \;=\; & \sqrt{\frac{2}{\pi w(z)^2\, 2^{m+n} m! n!}}\; H_m\left(\sqrt{2}\frac{x}{w(z)}\right) H_n\left(\sqrt{2}\frac{y}{w(z)}\right) \\ & \times\; \exp\left[-\frac{r^2}{w(z)^2} + ik\frac{r^2}{2R(z)} - i(m+n+1)\arctan\frac{z}{b} + ikz\right], \end{aligned} \tag{28}$$

where the functions $H_m(X)$ are the Hermite polynomials. Functions $w(z)$ and $R(z)$ are respectively the width parameter of the beam and curvature radius of the equiphase surface. After defining the constant $w(0) = w_0$ and the Rayleigh parameter $b = \pi w_0^2/\lambda$, those functions are given by

$$w(z) \;=\; w_0\sqrt{1+(z/b)^2}\,, \tag{29}$$

$$R(z) \;=\; z + b^2/z\,. \tag{30}$$

This is a model of the laser beam, diffracting with a width almost constant over a range shorter than the Rayleigh parameter, then linearly widening at infinity. The diffraction angle is

$$\theta = w_0/b = \lambda/\pi w_0,$$

and a smaller initial width (waist) causes larger diffraction angles. The curvature radius is infinite at $z = 0$ (flat wavefront), a minimum ($2b$) at the Rayleigh distance b and near a sphere of radius z at infinity (i.e. $z \gg b$). The normalized LG family is defined in polar coordinates by

$$\begin{aligned}\mathrm{LG}_{mn}(r,\phi) \;=\; & \sqrt{\frac{2\;m!}{\pi w(z)^2\,(m+n)!}}\; \left(\sqrt{2}\frac{r}{w(z)}\right)^n L_m^{(n)}\left(2\frac{r^2}{w(z)^2}\right)\exp(in\phi) \\ & \times\; \exp\left[-\frac{r^2}{w(z)^2} + ik\frac{r^2}{2R(z)} - i(2m+n+1)\arctan\frac{z}{b} + ikz\right], \end{aligned} \tag{31}$$

where the $L_m^{(n)}(X)$ are the generalized Laguerre polynomials. The set HG_{mn} (resp LG_{mn}) is an orthonormal and closed family.

The common feature of all these modes is their spherical wavefront. It is thus possible to match a spherical mirror to a given beam for reflecting it on itself. Conversely, with the length of the cavity being fixed and the curvature radius of the two mirrors being given, a resonant mode matching the

cavity may exist. Assume for instance a length L, a flat input mirror and an end mirror of curvature radius R. A mode matching the cavity must have a waist ($z = 0$) located on the input mirror; its curvature radius at $z = L$ is

$$R(L) = L + b^2/L = R.$$

Solving for b yields

$$b = \sqrt{L(R-L)},$$

showing that solutions exist for $R > L$. The width w_0 on the input mirror is

$$w_0 = \sqrt{\lambda b/\pi} = \sqrt{\frac{\lambda}{\pi}\sqrt{L(R-L)}},$$

whereas the width on the end mirror is

$$w_L = \sqrt{\frac{\lambda R}{\pi}\sqrt{\frac{1}{R/L-1}}}.$$

For the fundamental mode $\mathrm{TEM}_{00}(r) = \mathrm{HG}_{00}(r) = \mathrm{LG}_{00}(r)$, the relative light power outside a circle of radius a is given by

$$P(r > a, z) = \exp(-2a^2/w(z)^2).$$

If ϵ is the maximum allowed power falling outside a circular mirror, its diameter $2a$ must be such that

$$a > w(z)\sqrt{\ln\left(1/\sqrt{\epsilon}\right)}.$$

For $\epsilon = 10^{-7}$ (i.e. 0.1 ppm) this is $a/w \sim 2.84$ so that in order to store a mode of width $w = 2$ cm with negligible losses, a mirror of diameter 11.4 cm would be sufficient. In practice, mirrors used in GW interferometric detectors are much larger for other reasons (35 cm for Virgo).

4.4 Interferometry in a GW Background

A passing gravitational wave interacts with light, as seen above. Let us see in details how this is translated by the interferometer. Our light ray is in fact a monochromatic plane wave of frequency $\nu = \omega/2\pi$. Call $B(t)$ the (complex) amplitude at the end of the round trip, and $A(t)$ its value at the beginning. We have

$$B(t) = A(t_r).$$

If we note

$$A(t) = A\mathrm{e}^{-i\omega t},$$

we get

$$B(t) = A\mathrm{e}^{-i\omega t_r} = A\mathrm{e}^{-i\omega(t-2L/c)}\exp\left[ih\frac{\omega L}{c}\mathrm{sinc}(\Omega L/c)\cos\left(\Omega(t-L/c)\right)\right].$$

Since we are always at first order in h, we write

$$B(t) = A\mathrm{e}^{-i\omega t}\mathrm{e}^{2i\omega L/c} +$$

$$\tfrac{i}{2}hA\,\tfrac{\omega L}{c}\mathrm{sinc}(\Omega L/c)\,\mathrm{e}^{2i\omega L/c}\mathrm{e}^{i\Omega L/c}\mathrm{e}^{-i(\omega+\Omega)t} +$$

$$\tfrac{i}{2}hA\,\tfrac{\omega L}{c}\mathrm{sinc}(\Omega L/c)\,\mathrm{e}^{2i\omega L/c}\mathrm{e}^{-i\Omega L/c}\mathrm{e}^{-i(\omega-\Omega)t}.$$

It clearly appears that the action of the GW was to create two sidebands of very low amplitude, of frequencies $\nu \pm \nu_g$ from one single frequency ν. Now let us see what happens if the incoming optical wave is already modulated and exhibits two sidebands. This is necessary because in interferometers, light undergoes the action of the GW several times in order to enhance signal production. Let the incoming amplitude be of the form

$$A(t) = \left(A_0 + \frac{1}{2}\, h\, A_1 \mathrm{e}^{-i\Omega t} + \frac{1}{2}\, h\, A_2 \mathrm{e}^{i\Omega t} \right) \mathrm{e}^{-i\omega t}.$$

The scaling factor is h because we assume the GW to be the only cause of generation of sidebands in the whole (arbitrary) optical system. We have then

$$\begin{aligned} B(t) = A(t_r) \;=\; & \left[A_0 + \frac{1}{2} h A_1 \mathrm{e}^{-i\Omega t} \mathrm{e}^{2i\eta} + \frac{1}{2} h A_2 \mathrm{e}^{i\Omega t} \mathrm{e}^{-2i\eta} \right] \\ & \times\; \mathrm{e}^{-i\omega t} \mathrm{e}^{2i\xi} \mathrm{e}^{-i\epsilon h \xi \mathrm{sinc}(\eta) \cos(\Omega t - \eta)}\,. \end{aligned}$$

For shortening the formula, we have used the abbreviations $\xi \equiv \omega L/c$ and $\eta \equiv \Omega L/c$. After a first order expansion of the exponential, we get

$$B(t) = \left(B_0 + \frac{1}{2}\, h\, B_1 \mathrm{e}^{-i\Omega t} + \frac{1}{2}\, h\, B_2 \mathrm{e}^{i\Omega t} \right) \mathrm{e}^{-i\omega t},$$

with the following notation:

$$\begin{aligned} B_0 \;&=\; \mathrm{e}^{2i\xi} A_0, \\ B_1 \;&=\; \mathrm{e}^{2i(\xi+\eta)} A_1 - i\epsilon\xi \mathrm{sinc}(\eta) \mathrm{e}^{i(2\xi+\eta)} A_0, \\ B_2 \;&=\; \mathrm{e}^{2i(\xi-\eta)} A_2 - i\epsilon\xi \mathrm{sinc}(\eta) \mathrm{e}^{i(2\xi-\eta)} A_0. \end{aligned}$$

We see that if we define "generalized amplitudes" as rank three vectors having the carrier amplitude, with the upper sideband and the lower sideband respectively as coordinates, by setting

$$\mathcal{A} = (A_0,\ A_1,\ A_2),$$

and

$$\mathcal{B} = (B_0,\ B_1,\ B_2),$$

the amplitude after a round trip that we have previously computed may be written in the form

$$\mathcal{B} = \boldsymbol{X}\mathcal{A},$$

where $\boldsymbol{X}$ is the linear round trip operator defined as

$$\boldsymbol{X} = \begin{pmatrix} \mathrm{e}^{2i\xi} & 0 & 0 \\ -i\epsilon\xi \mathrm{sinc}(\eta) \mathrm{e}^{i(2\xi+\eta)} & \mathrm{e}^{2i(\xi+\eta)} & 0 \\ -i\epsilon\xi \mathrm{sinc}(\eta) \mathrm{e}^{i(2\xi-\eta)} & 0 & \mathrm{e}^{2i(\xi-\eta)} \end{pmatrix}. \tag{32}$$

It is easy to check that the set of all operators having the form

$$\boldsymbol{O} = \begin{pmatrix} O_{00} & 0 & 0 \\ O_{10} & O_{11} & 0 \\ O_{20} & 0 & O_{22} \end{pmatrix},$$

is stable for any algebraic operation, and may even be given the structure of a noncommutative field which means that it can be viewed as a set of ordinary numbers, except that the product is generally not commutative. We call it $\mathcal{S}$ for brevity. The basic algebraic operations are defined by $(a, b = 0, 1, 2;\ i, j = 1, 2)$

– The sum
$$(\boldsymbol{A}+\boldsymbol{B})_{ab} = \boldsymbol{A}_{ab} + \boldsymbol{B}_{ab}.$$
– The product by a complex number
$$(z\cdot\boldsymbol{A})_{ab} = z\,(\boldsymbol{A})_{ab}\,.$$
– The product
$$(\boldsymbol{AB})_{aa} = A_{aa}B_{aa},$$
$$(\boldsymbol{AB})_{i0} = A_{i0}B_{00} + A_{ii}B_{i0}.$$
– The inverse
$$(\boldsymbol{A}^{-1})_{aa} = \frac{1}{A_{aa}},$$
$$(\boldsymbol{A}^{-1})_{i0} = -\frac{A_{i0}}{A_{00}\,A_{ii}}.$$

An $\mathcal{S}$ operator may be associated with any optical element of a complex optical system. The diagonal terms $\boldsymbol{O}_{aa}$ represent action of that element on the carrier and the sidebands. Often (for mirrors and lenses) there is no frequency dependence because the gravitational perturbation causes a negligible frequency shift, well inside the tolerances of the mirror coatings, and in this case, the corresponding operator is simply a scalar. In fact, the only non-diagonal operators are those corresponding to propagation of light in a vacuum over long distances. The result is that, after some $\mathcal{S}$ algebra, the whole optical system has an associated $\mathcal{S}$ operator describing its behavior. This approach was first proposed by Vinet et al. (1988).

5 SIGNAL TO NOISE RATIO

We can start with a pure monochromatic wave
$$\mathcal{A}_{\rm in} = (A,\ 0\ ,0).$$
$\boldsymbol{S}$ is the system's $\mathcal{S}$ operator, and we know that the output wave is given by
$$\boldsymbol{A}_{\rm out} = A\,\left[S_{00} + \frac{h}{2}S_{10}\,{\rm e}^{-i\Omega t} + \frac{h}{2}S_{20}\,{\rm e}^{i\Omega t}\right]{\rm e}^{-i\omega t}.$$
The corresponding detectable power is, up to a normalization factor, and calling $P_{\rm in}$ the incoming power:
$$P(t) = \boldsymbol{A}_{\rm out}\,\overline{\boldsymbol{A}}_{\rm out}$$
$$= P_{\rm in}\left[|S_{00}|^2 + \frac{h}{2}\,\left(S_{10}\overline{S}_{00} + \overline{S}_{20}S_{00}\right){\rm e}^{-i\Omega t} + \frac{h}{2}\,\left(S_{20}\overline{S}_{00} + \overline{S}_{10}S_{00}\right){\rm e}^{i\Omega t}\right].$$
The signal amplitude at frequency ν_g is thus
$$S(\nu_g) = |S_{10}\overline{S}_{00} + \overline{S}_{20}S_{00}|.$$
The DC component of the output is proportional to $|S_{00}|^2$, so that our main concern, the SNR, is proportional to
$${\rm SNR}(\nu_g)\ \propto\ |S_{10}\,{\rm e}^{-i\varphi_{00}} + \overline{S}_{20}\,{\rm e}^{i\varphi_{00}}|,$$
where φ_{ab} is the argument of S_{ab}. We have as well, with the correct normalization
$${\rm SNR}(\nu_g) = \sqrt{\frac{P_{\rm in}}{2h_{\rm P}\nu}}\,||S_{10}| + |\overline{S}_{20}|\,{\rm e}^{i(\varphi_{10}+\varphi_{20}-2\varphi_{00})}|\,h(\nu_g). \qquad (33)$$

Inversely, the spectral density $h_{\rm SN}(\nu_g)$, equivalent to the quantum noise, is obtained by taking a unitary SNR

$$h_{\rm SN}(\nu_g) = \sqrt{\frac{2h_{\rm P}\nu}{P_{\rm in}}}\,\frac{|S_{00}|}{|S_{10}\overline{S}_{00} + \overline{S}_{20}S_{00}|}.$$

We see that evaluation of the SNR of any optical GW detector eventually reduces to calculation of the S_{i0} of the whole system.

5.1 Recycling Interferometers

5.1.1 Cavities

The first element we need, before addressing more complex structures, is the $\mathcal{S}$ operator associated with the Fabry-Perot (FP) cavity. We take the same notations as in Figure 5. The intracavity (vector) amplitude $\mathcal{B}$ obeys

$$\mathcal{B} = t_1\mathcal{A}_{\rm in} - r_1 r_2 \boldsymbol{X}\,\mathcal{B},$$

where $\boldsymbol{X}$ is the round trip operator just defined above (Eq. (32)). We have thus

$$\mathcal{B} = [1 + r_1 r_2 \boldsymbol{X}]^{-1}\; t_1\,\mathcal{A}_{\rm in}.$$

The reflected amplitude is

$$\mathcal{A}_{\rm ref} = i\,r_1\,\mathcal{A}_{\rm in} + i\,t_1 r_2\,\boldsymbol{X}\,\mathcal{B}$$
$$= i\;[r_1 + (1-p_1)r_2\,\boldsymbol{X}]\;[1 + r_1 r_2 \boldsymbol{X}]^{-1}\;\mathcal{A}_{\rm in},$$

so that the reflectance of the cavity is the operator

$$\boldsymbol{F} = [r_1 + (1-p_1)r_2\,\boldsymbol{X}]\;[1 + r_1 r_2 \boldsymbol{X}]^{-1}. \tag{34}$$

It is possible to compute the components of $\boldsymbol{F}$

$$\boldsymbol{F} = \begin{pmatrix} F & 0 & 0 \\ G_+ & F_+ & 0 \\ G_- & 0 & F_- \end{pmatrix}.$$

F is the ordinary reflectance of the FP for the carrier, and $F_\pm$ the ordinary reflectance of the FP for the upper and lower sidebands respectively. For the sake of simplicity, we again use the notation

$$\xi = kL,$$
$$\eta = \Omega L/c,$$

(recall that $\Omega/2\pi$ is the GW frequency). We then have, after direct evaluation of $\boldsymbol{F}$ according to Equation (34)

$$F = \frac{r_1 + (1-p_1)r_2 \mathrm{e}^{2i\xi}}{1 + r_1 r_2 \mathrm{e}^{2i\xi}},$$

$$F_\pm = \frac{r_1 + (1-p_1)r_2 \mathrm{e}^{2i(\xi\pm\eta)}}{1 + r_1 r_2 \mathrm{e}^{2i(\xi\pm\eta)}}, \tag{35}$$

$$G_\pm = -i\epsilon\,\frac{t_1^2 r_2 \xi \mathrm{sinc}(\eta)\mathrm{e}^{i(2\xi\pm\eta)}}{(1 + r_1 r_2 \mathrm{e}^{2i\xi})\left(1 + r_1 r_2 \mathrm{e}^{2i(\xi\pm\eta)}\right)}. \tag{36}$$

In the coupling rate (σ) formalism, this can be approximated by

$$F = -\frac{1 - \sigma + 2i\Delta f}{1 - 2i\Delta f}, \tag{37}$$

$$F_{\pm} = -\frac{1-\sigma+2i(\Delta f \pm f_g)}{1-2i(\Delta f \pm f_g)}, \tag{38}$$

$$G_{\pm} = i\epsilon\,\frac{2\mathcal{F}L}{\lambda}\,\frac{2-\sigma}{(1-2i\Delta f)\,[1-2i(\Delta f \pm f_g)]}, \tag{39}$$

where $\Delta f = \delta\nu/\delta\nu_{\rm FWHM}$ is the reduced detuning of the light source from resonance, and $f_g = \nu_g/\delta\nu_{\rm FWHM}$ is the reduced gravitational frequency. When we vary the detuning, we see that the modulus of G_+ has a resonance for $\Delta f = 0$ (resonance of the carrier) and a second resonance when the upper sideband becomes resonant, $\Delta f = -f_g$. The modulus of G_- also has a resonance for $\Delta f = 0$ and for $\Delta f = f_g$, when the lower sideband becomes resonant (see Fig. 6). A symmetrical figure can be obtained with $|G_+|$.

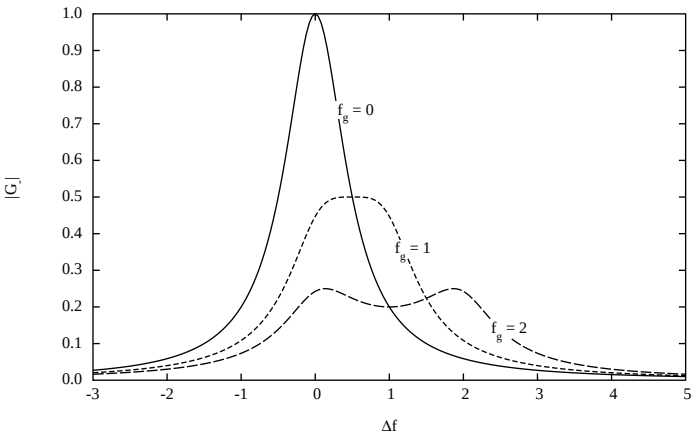

Fig. 6 Efficiency of lower sideband generation vs. detuning of the source for three reduced GW frequencies. Solid line: $f_g = 0$, short dashed line: $f_g = 1$, long dashed line: $f_g = 2$.

5.1.2 Michelson geometry

We take the classical Michelson geometry, but replace the end mirrors by two identical Fabry-Perot cavities, F_1 and F_2. Note that even when optically identical, the effect of a GW on them will be different, and consequently we must denote the corresponding operators by different notations (see Fig. 7). We neglect, in this first approach, small phases of order $2\pi\nu_g a/c$.

The transmitted amplitude is

$$\mathcal{A}_{\rm trans} = -r_s t_s \left(\mathrm{e}^{2ika}\boldsymbol{F}_1 + \mathrm{e}^{2ikb}\boldsymbol{F}_2\right)\,\mathcal{A}_{\rm in},$$

whereas the reflected amplitude is

$$\mathcal{A}_{\rm ref} = i\left(t_s^2\mathrm{e}^{2ika}\boldsymbol{F}_1 - r_s^2\mathrm{e}^{2ikb}\boldsymbol{F}_2\right)\,\mathcal{A}_{\rm in}.$$

Note that we neglect phases of the order of $2\pi\nu_g a/c$. The expressions of $\boldsymbol{F}_1$ and $\boldsymbol{F}_2$ for perfectly identical but orthogonal cavities, lying respectively along the x and y directions, are

$$\boldsymbol{F}_1 = \begin{pmatrix} F & 0 & 0 \\ G_+ & F_+ & 0 \\ G_- & 0 & F_- \end{pmatrix}, \quad \boldsymbol{F}_2 = \begin{pmatrix} F & 0 & 0 \\ -G_+ & F_+ & 0 \\ -G_- & 0 & F_- \end{pmatrix}.$$

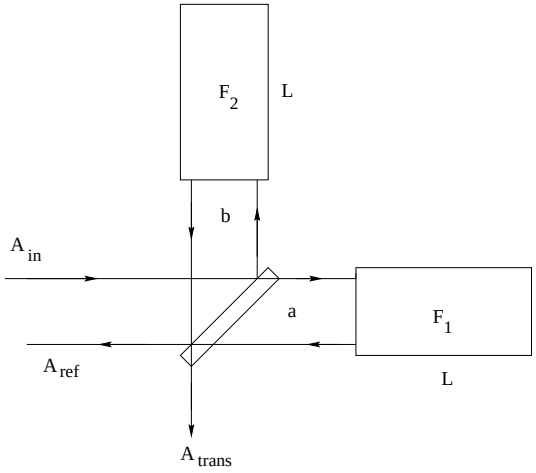

Fig. 7 Geometry of a Michelson Interferometer with FP cavities.

The opposite signs of the off-diagonal elements reflect the signature of a + polarized gravitational wave having the x, y axes as polarization directions. We can define a transmittance and a reflectance $\mathcal{S}$ operator in an obvious way, by

$$\mathcal{A}_{\rm trans} = \boldsymbol{T}_{\rm Mic}\, \mathcal{A}_{\rm in},$$
$$\mathcal{A}_{\rm ref} = i\, \boldsymbol{R}_{\rm Mic}\, \mathcal{A}_{\rm in}.$$

The elements of these operators are as follows, assuming a perfectly symmetrical splitter ($r_s = t_s = \sqrt{1-p_s}/2$), for the transmittance

$$T_{\rm Mic,00} = -(1-p_s)\mathrm{e}^{ik(a+b)}\cos[k(a-b)]\, F,$$
$$T_{\rm Mic,11} = -(1-p_s)\mathrm{e}^{ik(a+b)}\cos[k(a-b)]\, F_+,$$
$$T_{\rm Mic,22} = -(1-p_s)\mathrm{e}^{ik(a+b)}\cos[k(a-b)]\, F_-,$$
$$T_{\rm Mic10} = -i(1-p_s)\mathrm{e}^{ik(a+b)}\sin[k(a-b)]\, G_+,$$
$$T_{\rm Mic20} = -i(1-p_s)\mathrm{e}^{ik(a+b)}\sin[k(a-b)]\, G_-,$$

and for the reflectance

$$R_{\rm Mic,00} = i(1-p_s)\mathrm{e}^{ik(a+b)}\sin[k(a-b)]\, F,$$
$$R_{\rm Mic,11} = i(1-p_s)\mathrm{e}^{ik(a+b)}\sin[k(a-b)]\, F_+,$$
$$R_{\rm Mic,22} = i(1-p_s)\mathrm{e}^{ik(a+b)}\sin[k(a-b)]\, F_-,$$
$$R_{\rm Mic,10} = (1-p_s)\mathrm{e}^{ik(a+b)}\cos[k(a-b)]\, G_+,$$
$$R_{\rm Mic,20} = (1-p_s)\mathrm{e}^{ik(a+b)}\cos[k(a-b)]\, G_-.$$

It is evident that when the interferometer is tuned at a dark fringe for the carrier, the sidebands are transmitted, and conversely. The SNR takes the form

$$\mathrm{SNR}(\nu_g) \;\propto\; (1-p_s)\sin[k(a-b)]\, \left| G_+ \frac{\overline{F}}{|F|} - \overline{G}_- \frac{F}{|F|} \right|. \tag{40}$$

If we assume the carrier is at a dark fringe, we get

$$\boldsymbol{T}_{\rm Mic} = (1-p_s)\mathrm{e}^{ik(a+b)} \begin{pmatrix} 0 & 0 & 0 \\ -iG_+ & 0 & 0 \\ -iG_- & 0 & 0 \end{pmatrix}, \quad \boldsymbol{R}_{\rm Mic} = (1-p_s)\mathrm{e}^{ik(a+b)} \begin{pmatrix} iF & 0 & 0 \\ 0 & iF_+ & 0 \\ 0 & 0 & iF_- \end{pmatrix}.$$

This allows us to study the SNR of a simple Michelson interferometer having FP cavities as arms. We have in the coupling rate formalism, neglecting p_s at this level

$$\mathrm{SNR}(f_g) \;\propto\; \frac{4\mathcal{F}L}{\lambda}\,\frac{2-\sigma}{\sqrt{1+4\Delta f^2}}\,\frac{1}{2}\left|\frac{\mathrm{e}^{i\Psi_+}}{\sqrt{1+4(\Delta f+f_g)^2}}+\frac{\mathrm{e}^{-i\Psi_-}}{\sqrt{1+4(\Delta f-f_g)^2}}\right|,$$

where

$$\Psi_+ = \tan^{-1}\left(2(\Delta f+f_g)\right) - \tan^{-1}\left(\frac{2\Delta f}{1-\sigma}\right),$$

$$\Psi_- = \tan^{-1}\left(2(\Delta f-f_g)\right) - \tan^{-1}\left(\frac{2\Delta f}{1-\sigma}\right).$$

After some algebra, we find the following result

$$\mathrm{SNR}(f_g) \propto \frac{8(1-\sigma/2)\mathcal{F}L}{\lambda} \times \left[\frac{(1-\sigma+4\Delta f)^2+4(1-\sigma)^2 f_g^2}{(1+4\Delta f)^2\left((1-\sigma)^2+4\Delta f)^2\right)\left(1+8(\Delta f^2+f_g^2)+16(\Delta f^2-f_g^2)^2\right)}\right]^{1/2}, \quad (41)$$

if the cavities are at resonance ($\Delta f = 0$), we have simply

$$\mathrm{SNR}(f_g) = \frac{8\mathcal{F}L}{\lambda}\,\frac{1-\sigma/2}{\sqrt{1+4f_g^2}}\,\sqrt{\frac{P_{\rm L}}{2h_P\nu}}\,h(f_g).$$

We plot hereafter the spectral density of equivalent h for various values of $\mathcal{F}$ for a 20W light source at $\lambda = 1.064\,\mu\mathrm{m}$ (see Fig. 8). The sensitivity at low frequency is a function of $\mathcal{F}$. The optimum value of $\mathcal{F}$ theoretically occurs for $\sigma = 1$, i.e. for the optimal coupling of the cavities. This corresponds to $\mathcal{F} = \pi/p$. For $p = 3\times10^{-5}$, this corresponds to a finesse of 10^5.

On the other hand, when $\sigma = 1$, the surtension coefficient is $\mathcal{S} = 1/p$, and this means here a surtension of $\simeq 3\times10^4$. For a 10 W laser source, this is 0.3 MW of stored light power. However, let us keep in mind that the improvement due to increasing the finesse only occurs at low frequency. However, at low frequency, the limitation of the sensitivity is due to thermal noise, and it is worthless to try higher finesses as long as a means of reducing thermal noise has not been found. A better idea is to increase the laser power, because the whole curve is then globally lowered. However, 20W was available during the R&D phase, and the maximum presently reasonable for a CW monomode, stabilized laser. For gaining one order of magnitude in SNR, we would have had to lock an array of 100 such lasers in phase, which seemed hardly feasible. The same result can be achieved with a much more elegant and convenient solution, as explained hereafter. Let us remark that for given ν_g, the SNR is of the form

$$\mathrm{SNR} = \frac{8\pi L}{\lambda}\,\frac{1}{p}\,\frac{\sigma(1-\sigma/2)}{\sqrt{1+q^2\sigma^2}}\,\sqrt{\frac{P_{\rm L}}{2h_P\nu}}\,h(\nu_g),$$

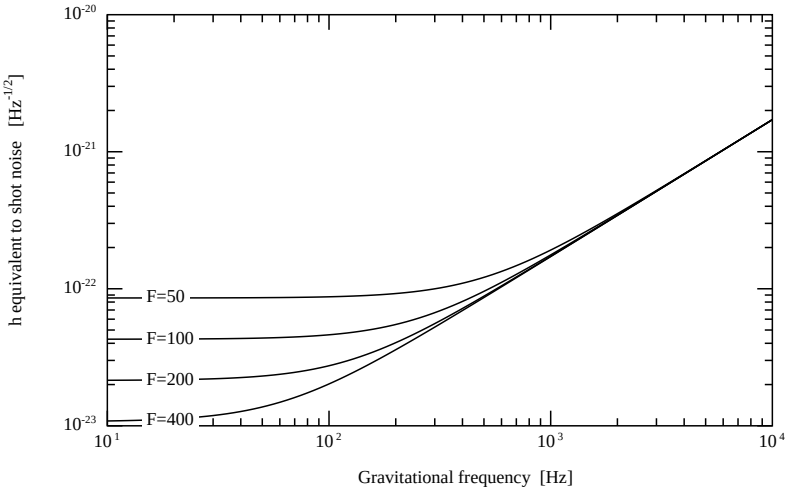

Fig. 8 Spectral density of h equivalent to shot noise.

with $q \equiv 2\pi\nu_g/p\Delta\nu_{\rm FSR}$ and consequently is a maximum for a finite value of σ. The parameter q is very high even for $\nu_g = 10\,\mathrm{Hz}$, and a good approximation of the optimal coupling rate is

$$\sigma_{\rm opt} = \left(\frac{2}{q^2}\right)^{1/3} = \left(\frac{p\Delta\nu_{\rm FSR}}{\sqrt{2}\,\pi\nu_g}\right)^{2/3}.$$

The optimal finesse is therefore

$$\mathcal{F}_{\rm opt}(\nu_g) = \left(\frac{\pi}{p}\right)^{1/3}\left(\frac{\Delta\nu_{\rm FSR}}{\nu_g}\right)^{2/3}.$$

For instance, with $p = 3\times10^{-5}$, $\Delta\nu_{\rm FSR} = 50\,\mathrm{kHz}$, this gives

$$\mathcal{F}_{\rm opt}(\nu_g) = 13782\times\left(\frac{10\mathrm{Hz}}{\nu_g}\right)^{2/3}.$$

However, the maximum is very flat, and it is not necessary to require the true optimum. A value of σ such that $q\sigma = 2$ is quite sufficient, with the SNR differing from its true optimum by only 10%. This corresponds to

$$\mathcal{F}_{\rm opt}(\nu_g) = \frac{\Delta\nu_{\rm FSR}}{\nu_g}.$$

The pseudo-optimal finesse for $\nu_g = 1$ kHz is for instance $\mathcal{F} = 50$. The pseudo-optimal finesse depends on a reference frequency $\nu_g^{(0)}$ which is an equivalent parameter, with the length of the cavities being fixed. In terms of this reference frequency, we have

$$\mathrm{SNR}(\nu_g) = \frac{4\,\frac{\nu_{\rm opt}}{\nu_g^{(0)}}}{\sqrt{1+\left(2\,\frac{\nu_g}{\nu_g^{(0)}}\right)^2}}\sqrt{\frac{P_{\rm L}}{2h_{\rm P}\nu}}h(\nu_g),$$

where $\nu_{\rm opt}$ is the optical frequency. This formula is valid except for too small values of $\nu_g^{(0)}$. For the interval [10 Hz, 10 kHz], it is valid. We see the huge scale factor provided by the cavities. When the

two cavities have a common detuning, the SNR is reduced, as can be read directly in Equation (41). But a resonance occurs when the upper sideband created by the GW becomes resonant (for $f_g = \Delta f$). At this frequency, the loss due to the frequency offset of the carrier is somewhat compensated by the resonance (see Fig. 9).

One important point is that, working out of resonance, the reflectances of the cavities are much higher than in the tuned case. This regime of operation, of no benefit in the simple Michelson configuration, becomes interesting when recycling is applied, as will be shown later.

It is clear from conservation laws in general, and namely from the previous section, that when tuned at a dark fringe, the transmittance of the Michelson interferometer is a minimum, while its reflectance is a maximum. It has been proposed a long time ago by R. Drever to build a cavity with one extra mirror (the recycling mirror) and the Michelson interferometer as a second mirror (see Fig. 10 for notation). By controlling the resonance of this *recycling cavity*, the surtension coefficient enhances the power reaching the splitter, and the SNR is increased.

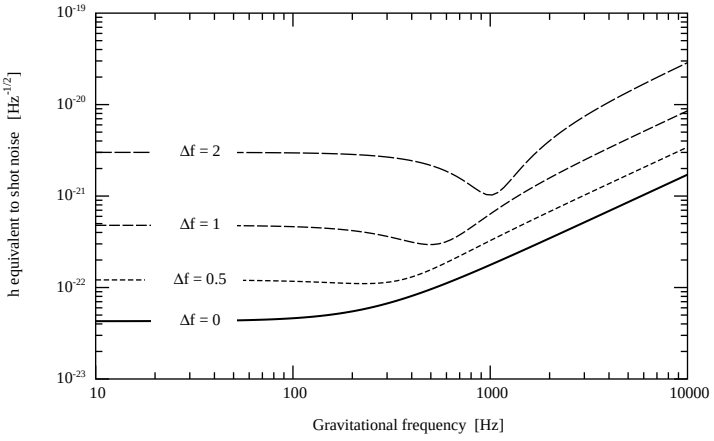

Fig. 9 Michelson Interferometer with detuned cavities ($F = 100$).

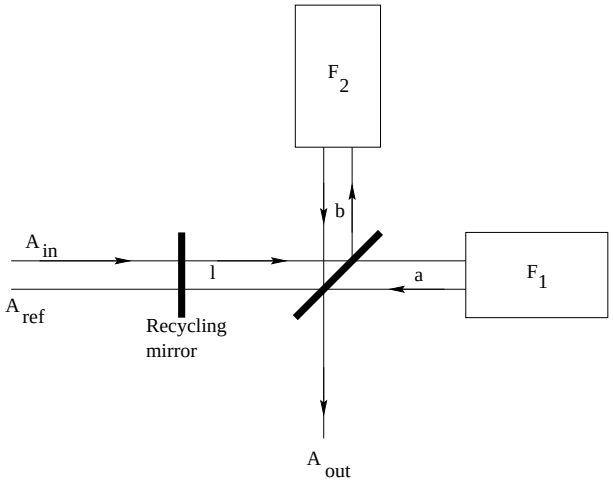

Fig. 10 Recycled Michelson Interferometer with FP cavities.

The $\mathcal{S}$ operator corresponding to this configuration is easily obtained by copying the simple Fabry-Perot operators. The Michelson operators for reflection and transmission are respectively $\boldsymbol{R}_{\rm Mic}$ and $\boldsymbol{T}_{\rm Mic}$, and l is the length of the recycling cavity, so we have for the reflectance and transmittance of the complete interferometer

$$\boldsymbol{R}_{\rm Itf} \;=\; \left[r_r + (1-p_r)\mathrm{e}^{2ikl}\boldsymbol{R}_{\rm Mic}\right]\,\left[1+\mathrm{e}^{2ikl}r_r\boldsymbol{R}_{\rm Mic}\right]^{-1}, \tag{42}$$

$$\boldsymbol{T}_{\rm Itf} \;=\; \mathrm{e}^{ikl}t_r\boldsymbol{T}_{\rm Mic}\left[1+\mathrm{e}^{2ikl}r_r\boldsymbol{R}_{\rm Mic}\right]^{-1}. \tag{43}$$

We are especially interested in the $T_{\mathrm{Itf}\ 10,20}$ components, giving the SNR. Using the preceding results about the Michelson operators, after some algebra, we obtain ($\delta \equiv k(a-b)$)

$$T_{\mathrm{Itf}\ 10,20} \;=\; -i\,\frac{t_r(1-p_s)\mathrm{e}^{ik(l+a+b)}\,G_{\pm}\left[\sin\delta + i\,r_r(1-p_s)\mathrm{e}^{ik(2l+a+b)}\,F_{\pm}\right]}{D\,D_{\pm}},$$

$$T_{\mathrm{Itf}\ 00} \;=\; -\,\frac{t_r(1-p_s)\mathrm{e}^{ik(l+a+b)}\,\cos\delta\,F}{D},$$

with the following definition ($a=-1,0,1$):

$$D_a = 1 + i\,r_r(1-p_s)\mathrm{e}^{ik(2l+a+b)}\sin\delta\,F_a.$$

It is always possible to tune the path difference between the two arms at a dark fringe ($\delta \equiv \pi/2[\mathrm{mod}2\pi]$), and the length l of the recycling cavity in order to obtain resonance, i.e.

$$D = 1 - r_r(1-p_s)\,|F|,$$

where F refers to the (assumed common) reflectance of the cavities. At this point, the SNR is simply the SNR of a Michelson interferometer, multiplied by the surtension factor

$$\mathrm{SNR}(f_g) = \mathrm{SNR}_{\rm Mic}(f_g) \times \frac{t_r}{1-r_r(1-p_s)\,|F|}. \tag{44}$$

In the so called *standard recycling* scheme, we assume the FP cavities are at resonance ($\Delta f = 0$). The SNR takes on the simple form

$$\mathrm{SNR} = \frac{4\frac{\mathcal{F}L}{\lambda}(2-\sigma)}{\sqrt{1+4f_g^2}}\;\frac{t_r(1-p_s)}{1-r_r(1-p_s)|1-\sigma|}\;\sqrt{\frac{P_{\rm L}}{2h_P\nu}}\;h(\nu_g),$$

where we directly see how increasing the coupling factor increases the Michelson SNR, but decreases the recycling factor. Anyway, we are free to choose the best recycling reflectance r_r, i.e. that maximizes the recycling surtension factor. This happens when

$$r_{r\mathrm{opt}} = (1-p_r)(1-p_s)|1-\sigma|,$$

giving

$$S_{r\mathrm{opt}} = (1-p_s)\sqrt{\frac{1-p_r}{1-(1-p_r)(1-p_s)^2(1-\sigma)^2}}\;\frac{4\frac{\mathcal{F}L}{\lambda}(2-\sigma)}{\sqrt{1+4f_g^2}}\;\sqrt{\frac{P_{\rm L}}{2h_P\nu}}\;h(\nu_g).$$

The mirror losses will be taken to be very small (on the order of 10 ppm), and we have seen that the coupling rate in a simple Michelson interferometer must be relatively small. It will be even smaller here, because the recycling factor would be destroyed by a large cavity absorption. It is therefore not

unrealistic to consider that the total losses are dominated by the cavity resonant absorptions, which are, however, small ($p_r + 2p_s \ll 2\sigma \ll 1$). The optimal SNR is then

$$\mathrm{SNR}(\nu_g) = \frac{4\pi L}{\sqrt{2}\lambda}\,\frac{1}{p}\,\frac{\sigma^{1/2}(2-\sigma)}{\sqrt{1+\left(2\pi\frac{\nu_g}{p\,\Delta\nu_{\mathrm{FSR}}}\,\sigma\right)^2}}\,\sqrt{\frac{P_{\mathrm{L}}}{2h_P\nu}}\,h(\nu_g).$$

When searching for the optimal value of σ, we get the following equation, with $q = 2\pi\nu_g/p\Delta\nu_{\mathrm{FSR}}$:

$$\frac{1}{2}q^2\sigma^3 + q^2\sigma^2 + \frac{3}{2}\sigma^2 - 1 = 0.$$

To avoid an exact but useless and cumbersome resolution of this equation, we would rather solve it in q

$$q^2 = \frac{1 - 3\sigma^2/2}{\sigma^2(1+\sigma/2)}.$$

Now we remark that, even for low GW frequencies (10 Hz), q^2 is very large. Consequently, σ must be very small, and we can take the approximation

$$\sigma_{\mathrm{opt}} = \frac{1}{q},$$

or, in terms of finesse,

$$\mathcal{F}_{opt} = \frac{\Delta\nu_{\mathrm{FSR}}}{2\nu_g^{(0)}},$$

where $\nu_g^{(0)}$ is the GW frequency at which the SNR is optimized. However, the maximum is sharp (see Fig. 11). Remark that this value is half the pseudo-optimum for the simple Michelson interferometer.

This sharp maximum makes the SNR very sensitive to the GW frequency at which the SNR is optimized.

With physically significant parameters (frequencies in the detection range [10 Hz, 10 kHz], and small losses), the SNR can be approximated by a simple formula. Call p_{ITF} the losses encountered in the recycling mirror and the splitter, i.e. the losses external to the FP's, then we have

$$1 - p_{\mathrm{ITF}} = (1-p_r)(1-p_s)^2 \;\Rightarrow p_{\mathrm{ITF}} \;\simeq\; p_r + 2p_s.$$

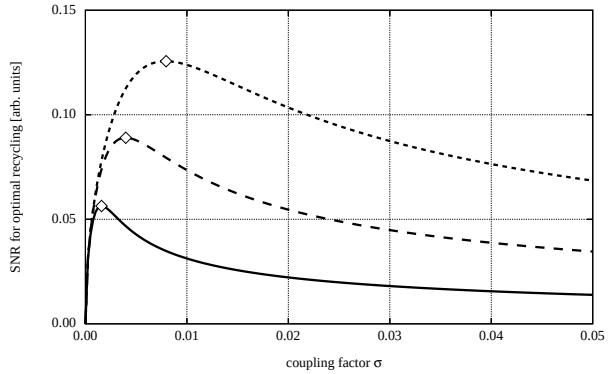

Fig. 11 SNR vs. σ for three GW frequencies. The small diamonds show the approximate theoretically derived optima.

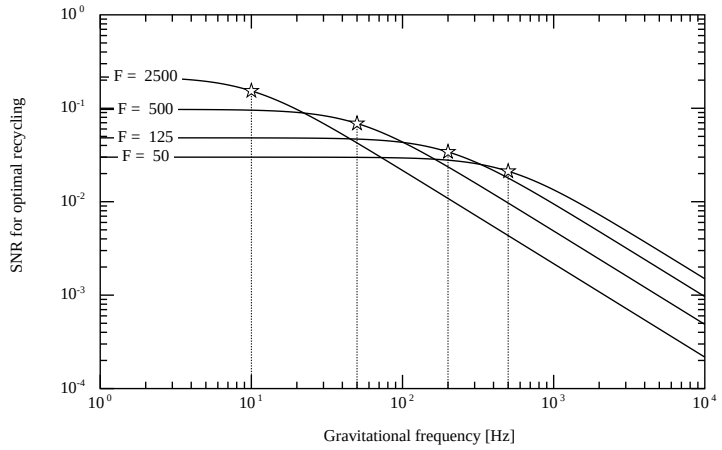

Fig. 12 SNR vs. frequency for four finesses. The small stars point to the GW frequency at which the SNR was optimized.

The losses internal to the FP's are still $p = 1 - (1 - p_1)r_2^2$. Neglecting non essential small terms leads to

$$\mathrm{SNR}(\nu_g) = \frac{1}{\sqrt{p_{\mathrm{ITF}} + \frac{p\Delta\nu_{\mathrm{FSR}}}{\pi\nu_g^{(0)}}}} \frac{2\frac{\nu_{\mathrm{opt}}}{\nu_g^{(0)}}}{\sqrt{1 + \left(\frac{\nu_g}{\nu_g^{(0)}}\right)^2}} \sqrt{\frac{P_{\mathrm{L}}}{2h_{\mathrm{P}}\nu}}\, h(\nu_g), \tag{45}$$

the parameter $p\Delta\nu_{\mathrm{FSR}}/2\pi$ has the dimension of a frequency, and is on the order of 1 Hz. The first term represents the gain due to optimal recycling, and the second is the SNR of a simple Michelson. We can conclude that a power recycled Michelson scheme, having an optimal recycling rate, and an optimal finesse at a given GW frequency, is not significantly better than that of a simple Michelson scheme when the frequency is very low. In this subsection and in the next one, we see how the reflectivity of the Fabry-Perot cavities play a central role. The efficiency of recycling crucially depends on the quality of the reflectivity. This is the reason why at low frequency, a high finesse is needed, the coupling rate increases, the reflectivity decreases, and the effect of recycling becomes negligible. This strong requirement of very reflective cavities was the cause of a number of numerical optics studies that, in turn, motivated Section 3.

The amplitude in the recycling cavity has a peak at the recycling resonance. It is interesting to evaluate the width of the resonance line when the frequency of the source varies. The surtension factor reads

$$S_r = \left| \frac{t_r}{1 + ir_r(1 - p_s)\,\mathrm{e}^{ik(2l+a+b)} \sin\delta F} \right|^2 .$$

In this expression, the dominating phase is obviously given by the reflectance F. Since the phase reflected by cavities already has a sharp slope, we can expect this slope to be reinforced by the recycling finesse. We can take for the modulus of the reflectance its value $|F| = 1 - \sigma$ at resonance, and assume $\delta = \pi/2$ and $\pi/2 + k(2l + a + b) \equiv \pi$. The only frequency dependent quantity (in this approximation) is the phase Φ of the reflectance, given by

$$\Phi \sim 2\tan^{-1}(2\Delta f),$$

where we have assumed a small σ. If the frequency excursion is small compared to the cavity linewidth, then Δf is small, so that we can write

$$S_r = S_r^{(0)} \left| \frac{1}{1 + (4\mathcal{F}_R \Delta f/\pi)^2} \right|^2,$$

where $S_r^{(0)}$ is the peak height for a given detuning of the dark fringe δ, Δf is the reduced frequency excursion, and

$$\mathcal{F}_R = \frac{\pi\sqrt{r_r(1-p_s)(1-\sigma)\sin\delta}}{1 - r_r(1-p_s)(1-\sigma)\sin\delta},$$

the recycling finesse. This finesse obviously depends on the tuning of the Michelson interferometer. Detuning reduces the reflectance of the Michelson interferometer, as can be seen in Figure 13.

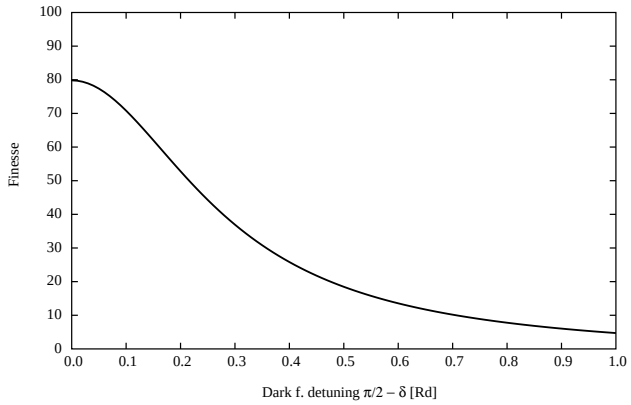

Fig. 13 Variable finesse by detuning the dark fringe.

The full width at half maximum of the surtension peak can therefore be estimated by

$$\delta\nu_{\rm rec} = \frac{\pi}{2\mathcal{F}_R}\,\delta\nu_{\rm FWHM}$$

(recall that $\delta\nu_{\rm FWHM}$ is the linewidth of the cavity). For standard values, say $p_s = 2 \times 10^{-5}$, $S_r^{(0)} = 50$, and hence $r_r = 0.962$, $\sigma = 6.366 \times 10^{-4}$, (corresponding to a cavity finesse of 50), we find $\mathcal{F}_R \sim 78$. For a 3 km long and 50 finesse cavity, the linewidth is 1 kHz, so that

$$\delta\nu_{\rm rec} \sim 20\,{\rm Hz},$$

which is very near the exact value, numerically obtained, of 19.64 Hz (in Fig. 14, we show the exact line shape for such parameters).

It is also clear that a detuning with respect to the dark fringe ($\delta \neq \pi/2$) not only decreases the maximum recycling gain, but also increases the recycling linewidth. In Figure 15, the full width at half maximum of the recycling width is plotted. This helps in tuning the interferometer.

5.2 Some Technological Issues

5.2.1 Vacuum

The interferometer must operate in a vacuum in order to avoid index fluctuations. The pressure level consistent with the phase noise budget is about 10^{-7} Torr. The entire system is therefore installed

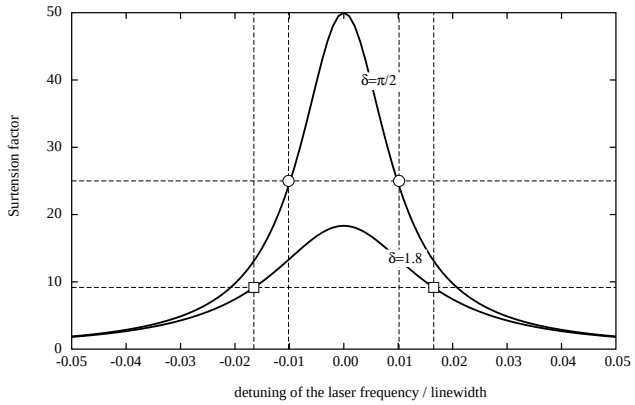

Fig. 14 Linewidth of the recycling cavity / linewidth of the long cavities. A detuning wrt dark fringe increases the recycling width.

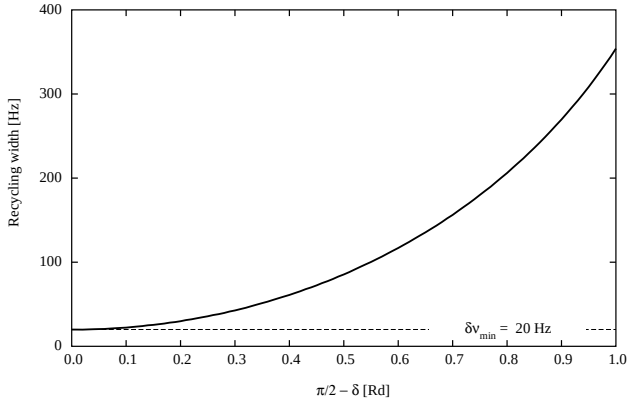

Fig. 15 Linewidth of the recycling cavity vs. dark fringe detuning $\delta \equiv 2\pi(a-b)/\lambda$.

in a vacuum tank involving two long pipes and a series of tanks in the central part, housing the suspensions of the various mirrors. In the case of Virgo, we thus have a series of eight towers. For keeping such a low pressure without continuous pumping, it is necessary to have a very low outgassing rate, and consequently to process the steel of the tubes by heating in such a way that the trapped hydrogen is extracted. After one initial pumping, the pressure is then practically stable for months, possibly needing the action of (silent) getter pumps from time to time.

5.2.2 Laser stabilization

Even highly stable lasers have frequency noise. If we call $\psi(t)$ the phase of the output light, the interference of the splitter after reflection by two arms of lengths a and b has the differential phase

$$\Psi(t) = \psi(t-2a/c) - \psi(t-2b/c) \;\sim\; \frac{2(b-a)}{c}\,\frac{\partial\psi}{\partial t}(t) = \frac{\Delta L}{L}\,\frac{4\pi L}{c}\delta\nu(t),$$

where L is the mean arm length and ΔL the length asymmetry. It is now clear that the phase noise resulting from the laser frequency fluctuations is proportional to the length asymmetry. For a simple short Michelson interferometer, it is possible to carefully tune the lengths in order to cancel a possible asymmetry. For a giant interferometer involving Fabry-Perot cavities, the source of asymmetry is mainly due to the difficulty of making identical cavities (i.e. mirrors having identical reflectances). We must take into account some irreducible finesse asymmetry $\Delta\mathcal{F}$, so that we can replace the L in the preceding formula by the effective length $2\mathcal{F}L/\pi$, and the $\Delta L/L$ by a $\Delta\mathcal{F}/\mathcal{F}$. Turning to linear spectral densities, this gives

$$S_\Psi(f)^{1/2} = \frac{\Delta\mathcal{F}}{\mathcal{F}}\,\frac{8\mathcal{F}L}{c}\,S_\nu(f)^{1/2},$$

where $S_\nu(f)$ is the PSD of laser frequency noise. On the other hand, the phase noise due to shot noise is known to be

$$S_{\Psi,\mathrm{sn}}(f)^{1/2} = \sqrt{\frac{2\hbar\omega}{P_{\mathrm{spl}}}},$$

where P_{spl} is the light power reaching the splitter. A requirement on the laser stability is obtained by demanding that the resulting phase noise be less than the shot noise induced phase noise. The condition is

$$\frac{S_\nu(f)^{1/2}}{\nu_0} < \frac{\lambda}{8\mathcal{F}L}\,\frac{\mathcal{F}}{\Delta\mathcal{F}}\,\sqrt{\frac{2\hbar\omega}{P_{\mathrm{spl}}}} \tag{46}$$

with parameters such that $\mathcal{F} = \triangledown\prime$, $L = 3\,\mathrm{km}$, $P_{\mathrm{spl}} = 1\,\mathrm{kW}$, and $\lambda = 1\,\mu\mathrm{m}$; this gives

$$S_\nu(f)^{1/2} < \frac{5\times10^{-9}}{\Delta\mathcal{F}/\mathcal{F}}\,\mathrm{Hz}\cdot\mathrm{Hz}^{-1/2},$$

so that with a finesse asymmetry, the requirement would be on the order of

$$S_\nu(f)^{1/2} < 5\times10^{-7}\,\mathrm{Hz}\cdot\mathrm{Hz}^{-1/2}.$$

Such a demanding stability requirement was satisfied in Virgo by a system of servo loops. A first pre-stabilization system uses a standard reference short cavity. A second loop involves one of the two arms of the interferometer as a short term reference.

5.2.3 Seismic isolation

The real motion of the mirrors would obviously compete directly with the effect of a gravitational wave signal. It is therefore necessary to suppress any transmission of the ground's permanent motion (seismic noise) to the mirrors. A measurement of the seismic noise linear spectral density on the Virgo site typically gives

$$S_x(f)^{1/2} = 10^{-8}\left[\frac{10\mathrm{Hz}}{f}\right]^2\ \mathrm{mHz}^{-1/2}.$$

An original isolation system has been conceived for the Virgo antenna. The idea is to use the benefit of the transfer function of the simple pendulum for motion of its suspension point. Let us call $x(t)$ the displacement of the suspension point, and $y(t)$ the resulting displacement of the mirror. We have the following transfer function:

$$\mathcal{T}(f) \equiv \frac{\tilde{y}(f)}{\tilde{x}(f)} = \frac{1}{(f/f_0)^2 - 1},$$

where f_0 is the resonance frequency of the pendulum. It is therefore clear (and well known) that the pendulum has a strong filtering effect for frequencies much larger than the resonance. If a resonance frequency of 0.1 Hz can be achieved, one sees that the attenuation factor is already 10^4 at 10 Hz. In principle, a chain of such pendulums will combine the elementary transfer functions in a multiplicative way, so that a chain of n pendulums would have roughly a transfer function mainly of the form

$$\mathcal{T}_n(f) = \left[\frac{1}{(f/f_0)^2 - 1}\right]^n \sim (f_0/f)^{2n} \text{ for } f \gg f_0.$$

Such a cascade of filters has been achieved for Virgo and is called a "superattenuator." It consists of five masses being able to move in the transverse direction by suspension wires and longitudinally as well due to welding of those wires on blade springs. The chain is itself suspended on an elastic structure called an "inverse pendulum" (see Fig. 16).

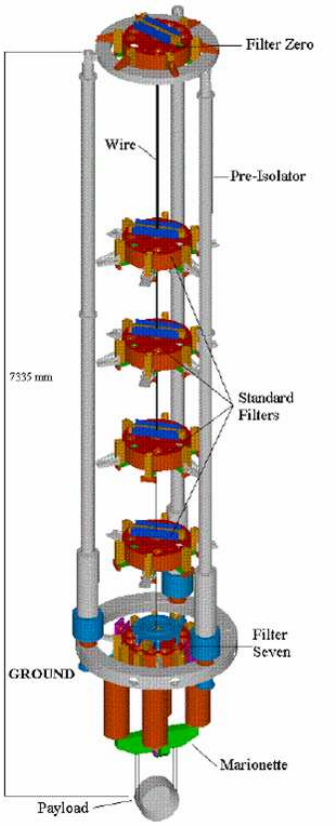

Fig. 16 "Superattenuator" at Virgo (see the site of EGO).

5.2.4 Dielectic mirrors

We have seen that power recycling is an essential point for reaching the target sensitivity. It has been shown that the recycling rate depends mainly on the reflectance of the long Fabry-Perot cavities which in turn is given by the coupling coefficient $\sigma \equiv p\mathcal{F}/\pi$. For a fixed finesse, the coupling coefficient is thus determined by the total losses p in the cavity. Those losses represent the part of the

Fig. 17 Large coating instrument at the site of the Laboratoire des Milieux Avancés (Nuclear Physics Institute of Lyon, France).

light power that is either thermalized on the mirrors' surfaces or coupled into modes different from the nominal TEM. Implementation of mirrors must therefore satisfy several strong requirements. Among them

- The surface must match the ideal wavefront. This means that the polishing phase must achieve a very good geometry. In order to get figures, a simulation program (now known as "DarkF," (Brillet et al. 2003)), able to represent diffraction of light and its reflection on imperfect surfaces, has been written in the Virgo collaboration, giving a requirement of about $\lambda/100$ for the geometrical defects on the central area of the mirrors. Only a few companies are able to obtain this result on large silica blanks.
- The input mirrors are crossed by the light beam and the thermalization in the bulk must be kept as low as possible. This requires a special synthetic silica of the same kind as the one used for optical fibers. On the other hand, any inhomogeneity in the refractive index results in a distortion of the emerging wavefront. A special synthetic silica has been elaborated giving an attenuation factor of about a few ppm/cm, with a special manufacturing protocol insuring the required homogeneity.
- The absorption of light on the internal surfaces of the Fabry-Perot cavities is a crucial issue. Losses smaller than a ppm require dielectric mirrors. If the wavelength of light is fixed ($\lambda \sim$ 1064 nm for the Nd: YAG laser), the properties of Fabry-Perot cavities at antiresonance can be exploited. Ignoring losses, a cavity involving mirrors of reflectances r' and r'' tuned at antiresonance has a global reflectance of

$$r = \frac{r' + r''}{1 + r'r''}.$$

  It is easily seen that $r > \max(r', r'')$, so that by building a stack of cavities, it is possible to reach any reflection coefficient by suitably choosing the number of elementary cavities. On the other hand, we know that the reflection index from a medium of index n_1 on a medium of index n_2 is

$$r = \frac{n_1 - n_2}{n_1 + n_2}.$$

The idea is thus to deposit layers of doped silica of thickness $\lambda/4$ with alternating "high" and "low" indices on the mirror substrate. The elementary reflectance of a single doublet of layers is typically on the order of $r_1 \sim 0.2$. According to the formula, with two doublets, the reflectance is already $r_2 \sim 0.38$, $r_3 \sim 0.54$ with three doublets, and so on. The complete stack giving the right global reflectance is called the "coating." Coatings having reflectance defects less than 1 ppm have been achieved.

The way of obtaining such very low absorption rates and high reflectivities is to combine a very high cleanliness of the coating facility (protecting from contamination of the deposit) with a very homogeneous deposition process and an accurate control of the thickness of the layers. Mastering such requirements on large silica substrates was a challenge. A special facility (see Fig. 17) has been built in Lyon (France) for this purpose[3].

5.2.5 Thermal noise

The mirror surfaces are the reference for the optical readout beam. Any spurious displacements of those surfaces directly compete with the gravitational wave signal. Since the seismic motions are attenuated by the suspension scheme, an extra source of perturbation remains at room temperature, due to random motion of matter in the substrate holding the reflecting surface. The substrate may be regarded as an elastodynamical resonator, and the motion of matter inside may be regarded as a superposition of eigenmodes of vibration.

There is a general derivation of the spectral density of thermal noise, based on the Fluctuation-Dissipation Theorem (FD), due to Callen & Welton (1951): for an elementary dynamical system described by a degree of freedom x and any driving force F, one can consider the resulting velocity $\tilde{v} = i\omega\tilde{x}$, and compute a mechanical impedance as $Z = \tilde{v}/\tilde{F}$. Then, this is the FD theorem

$$S_x(f) = \frac{4k_B T}{\omega^2} \Re e[Z], \tag{47}$$

where T is the temperature, k_B the Boltzmann constant and $\omega \equiv 2\pi f$. We can now address the problem of internal degrees of freedom in the mirrors. Internal elastic waves eventually distort the reflecting surface, causing a phase noise. We have the information on the surface motion relevant for the beam. Let $u_z(t, x, y)$ be the z component of the displacement vector of matter at the surface of the mirror. One can show that the equivalent global displacement (generalized coordinate x) is

$$x(t) = \iint u_z(t, x, y)\, I(x, y)\, dx\, dy,$$

where $I(x, y)$ is the normalized light intensity distribution in the TEM_{00} mode, assumed to be the readout beam. In other words, the equivalent global displacement is nothing but the average of the surface distortion, weighted by the readout beam intensity. We now follow the method proposed by Levin (1998). Let $F(t)$ be the corresponding driving force. The interaction energy is

$$\mathcal{E} = -F(t)\, x(t),$$

or

$$\mathcal{E} = \iint u_z(t, x, y) \boldsymbol{F}(t) \boldsymbol{I}(x, y)\, dx\, dy,$$

where the displacement u may be thought of as being caused by the pressure distribution $\boldsymbol{F} \times \boldsymbol{I}$. We now address the case of low frequencies. This case is very relevant, because resonances of mirrors are at relatively high frequencies (several kHz) and the region where internal thermal noise causes

[3] *http://lma.in2p3.fr*

disturbances lies long before the first resonance, in the low frequency regime. Thus, although some general knowledge of internal thermal noise is useful, it is nevertheless extremely interesting to have the low frequency tail. This can be obtained as follows. If we consider a force $F(t) = F\mathrm{e}^{i\omega t}$ oscillating at very low frequency, the frequency will be lower than the cut-off for any standing waves. The pressure $\boldsymbol{F} \times \boldsymbol{I}$ will produce an oscillating stationary displacement u of the form

$$u_z(t, x, y) = \mathrm{e}^{i(\omega t - \phi)} u(x, y),$$

which is equivalent to neglecting inertial forces in the motion of matter. The phase ϕ represents a retardation effect that dissipation may cause. In the Fourier domain, this is

$$u_z(\omega, x, y) = (1 - i\phi) u_z(x, y).$$

The impedance is

$$Z(f) = i\omega \, \frac{(1 - i\phi) \int\int u_z(x, y) \, I(x, y) \, dx \, dy}{F},$$

so that

$$\Re e[Z] = \omega \, \phi \, \frac{\int\int u_z(x, y) \, \boldsymbol{F} \cdot \boldsymbol{I}(x, y) \, dx \, dy}{F^2},$$

where the numerator of the fraction appears as the elastic energy stored in the solid stressed by the pressure distribution $\boldsymbol{F} \cdot \boldsymbol{I}$. The strain energy is defined in classical elasticity theory by

$$W = \frac{1}{2} \int\int u_z(x, y) p(x, y) \, dx \, dy,$$

where $p(x, y)$ is the pressure distribution causing the displacement $u_z(x, y)$ at the surface where it is applied. We can thus write for the spectral density of displacement

$$S_x(f) = \frac{4k_B T}{\pi f} \, \phi \, \frac{W}{F^2}.$$

In fact, W is proportional to F^2, so that $U \equiv W/F^2$ is the strain energy for a static pressure normalized to 1 N. The SD of displacement takes the general (low frequency) form

$$S_x(f) = \frac{4k_B T}{\pi f} \, \phi \, U. \tag{48}$$

The problem is reduced to the computation of U. This can be difficult in the general case of an arbitrary solid, but numerical finite element codes are able to give more or less accurate estimates. It is however possible to obtain analytic solutions in the case of axial symmetry. It has been shown in Bondu et al. (1998) that if we consider the mirror substrate as a semi-infinite medium (half a space limited by the reflecting surface), the strain energy U is simply

$$U = \frac{1 - \sigma^2}{2\sqrt{\pi} Y w},$$

where Y is the Young modulus of the material, σ its Poisson ratio and w the width of the beam (assuming TEM_{00}). At room temperature, these parameters are for silica $Y \sim 7.3 \times 10^{10} \mathrm{Nm}^{-2}$ and $\sigma \sim 0.17$. If we assume a width $w = 2\,\mathrm{cm}$ and a loss angle (inverse of a quality factor) $\phi \sim 10^{-6}$, we get a strain energy of

$$U_\infty \simeq 1.89 \times 10^{-10} \, \mathrm{JN}^{-2},$$

so that the low frequency tail of the thermal noise PSD is

$$S_x(f) \simeq 10^{-38} \left[\frac{100\,\mathrm{Hz}}{f} \right] \mathrm{m}^2 \, \mathrm{Hz}^{-1}.$$

In terms of an equivalent linear density of h, this is, taking the Virgo size ($L = 3\,\mathrm{km}$)

$$h(f) = \frac{2S_x(f)^{1/2}}{L} \simeq 6.65 \times 10^{-23}\ \mathrm{Hz}^{-1/2}.$$

This is the main limitation in sensitivity in the very important region of 100 Hz. Owing to this strategic context, a more accurate theory has, therefore, been developed for taking into account the finite size of the mirrors, and making it possible to study the effect of the aspect ratios on the PSD of thermal noise. The result is the BHV model (Bondu et al. 1998). In the case where both the mirrors and the beam are assumed to be axisymmetrical, there exists a model allowing an accurate calculation of the strain energy.

Let us summarize the results. The total internal energy is the sum of two contributions

$$U = U_0 + \Delta U,$$

that can be computed separately. Let a be the radius of the mirror and h its thickness. Let $J_\nu(x)$ be the Bessel functions and $\{\zeta_k,\ k > 0\}$ the family of all non-zero solutions of $J_1(\zeta) = 0$. Let us note $x_k \equiv \zeta_k h/a$ and $q_k \equiv \exp(-2x_k)$. Let Y be the Young modulus of the mirror's material and σ its Poisson ratio.

Then we have

$$U_0 = \frac{1-\sigma^2}{\pi a Y} \sum_{k>0} \frac{J_0^2(\zeta_k) p_k^2}{\zeta_k} \frac{1 - q_k^2 + 4q_k x_k}{(1-q_k)^2 - 4q_k x_k^2}. \tag{49}$$

The dimension of U is JN^{-2}.

In the preceding expression, the Fourier-Bessel coefficients $\{p_k,\ k > 0\}$ are determined by the pressure profile. If we denote this pressure distribution by $p(r)$, we have

$$p_k = \frac{2\pi}{J_0^2(\zeta_k)} \int_0^a p(r) J_0(\zeta_k r/a)\, r\, dr. \tag{50}$$

For the second contribution, we have

$$\Delta U = \frac{a^2}{6\pi h^3 Y} \left[\left(\frac{h}{a}\right)^4 + 12\sigma\xi \left(\frac{h}{a}\right)^2 + 72(1-\sigma)\xi^2 \right], \tag{51}$$

with

$$\xi \equiv \sum_{k>0} p_k J_0(\zeta_k)/\zeta_k^2.$$

At this level, the computation amounts to finding p_k. The general expression of the Fourier-Bessel coefficients for any LG mode has been given in Mours et al. (2006)

$$p_{k,m}^{(n)} = \frac{1}{J_0(\zeta_k)^2} \exp\left[-\frac{\zeta_k^2 w^2}{8a^2}\right] L_m^{(0)}\left(\frac{\zeta_k^2 w^2}{8a^2}\right) L_{n+m}^{(0)}\left(\frac{\zeta_k^2 w^2}{8a^2}\right).$$

For example, the Virgo mirrors have radius $a = 17.5\,\mathrm{cm}$ and thickness $h = 10\,\mathrm{cm}$. The width of the input mirror is $w = 2\,\mathrm{cm}$. An LG_{00} mode causes a virtual strain energy of

$$U \simeq 2.01 \times 10^{-10}\ \mathrm{JN}^{-2},$$

slightly worse than the semi-infinite approximation U_∞. Now, if we rearrange the cavities for using LG_{55} modes of width $w = 3.5\,\mathrm{cm}$, the strain energy becomes

$$U \simeq 8.64 \times 10^{-12}\ \mathrm{JN}^{-2},$$

which leads to a gain of about five in sensitivity. This seems to provide a way of escaping the thermal noise limitation without cryogenic facilities.

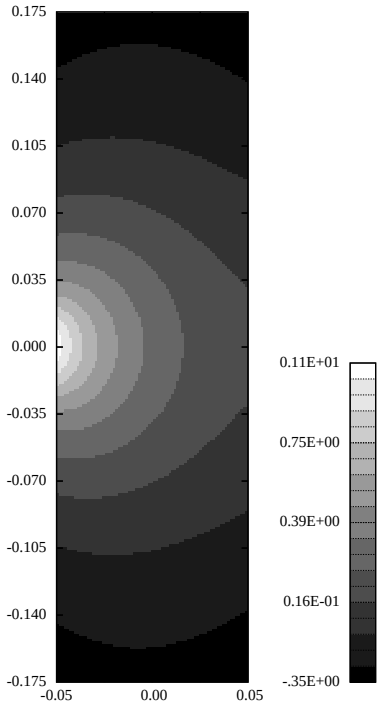

Fig. 18 Temperature field in a Virgo substrate for 1 W dissipated in the coating. Mode TEM00, $w = 2$ cm. (Logarithmic scale). From Vinet (2009).

5.2.6 Spurious thermal effects

If mirror thermal noise is reduced in any way, it becomes useful to increase the light power reaching the splitter, because it will increase the SNR in the crucial region around 100 Hz. However, even very low loss mirrors thermalize a fraction of the light power. If MW of light power are stored in the long cavities, there will be a source of heat on each mirror surface on the order of 1W. Heating the mirrors results in two effects.

- Due to the temperature dependence on the refraction index of the material (e.g. silica), an index field develops inside the substrate, reproducing the temperature field generated by the heat source, which has the profile of the optical beam intensity. The result is what is called a "thermal lens," which changes the optical properties of the whole system. See, for instance on Figure 18, the temperature or refractive index field, inside a substrate (35 cm diameter, 10 cm thick) heated on its surface by a 1 W heat source.
- The temperature field induces a strain field and a global deformation of the mirror's surface, again changing its optical properties. In Figure 19, one can see the effects of heat deformation on the same mirror, for three kinds of beams.

Several ideas have been explored for reducing or correcting these spurious effects. The first idea is to change the geometry of the readout beam in order to spread the light power over a wider area: one retrieves the same idea as for the thermal noise (preceding section). Flat profile beams and higher order modes have been proposed. The second idea is to correct the lens-

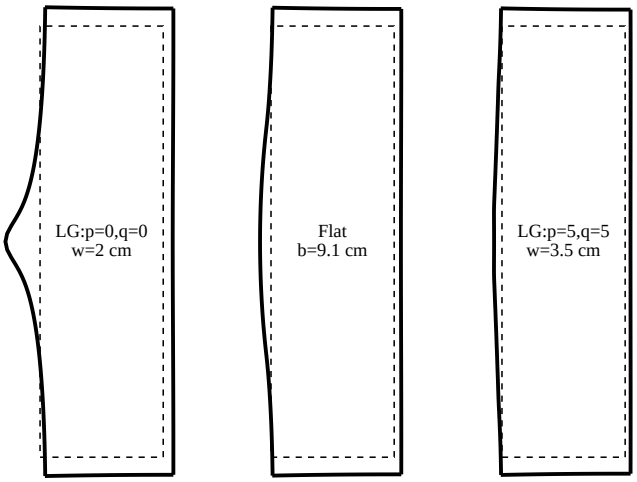

Fig. 19 Thermal deformation of a Virgo mirror under three types of readout beams (1 W absorbed in the coating, and exaggerated by a factor of 2×10^5). From Vinet (2009).

ing and/or the deformation by heating the cold regions of the mirror in order to reduce the temperature gradients. An extensive review of these ideas can be found in Vinet (2009). See also *http://www.icra.it/MG/mg12/talks/gw2_dipaolo.pdf* for a description of experimental work.

5.3 Pioneering Small Scale Antennas

Since the first laser interferometer antenna (5 m arm length) was built in the Hughes Lab by R. L. Forward (Forward 1978) in the sixties, at a time when gravitational wave amplitudes were poorly estimated, European and American groups have developed prototypes of several tens of meters for testing new optical ideas. The group of Glasgow University developed ideas around Fabry-Perot cavities, and a group from Garching (Max Planck Institüt) used multipass cells (Schnier et al. 1997). A collaboration between the two groups led to the GEO600 project, a Michelson interferometer with folded arms, of length 600 m, which was built in 1995 (Abbott et al. 2004) near Hannover (Germany). Simultaneously, a Japanese group (National Astronomical Observatory) constructed TAMA300 (a 300 m arm, power recycled Michelson interferometer)[4] in the vicinity of Tokyo. Two years later, a group from the University of Western Australia began the construction of a first step towards a larger antenna, namely an 80 m Michelson Interferometer in the vicinity of Perth[5]. All these instruments have proved useful for testing various original solutions to pending problems. For instance, monolithic suspension systems, i.e. suspension of silica mirror substrates by silica fibers, have been tested at Glasgow and have been shown to reduce the internal dissipation and strongly reduce the suspension thermal noise. Another example is the signal recycling (Meers 1988) scheme, demonstrated at GEO600, which enables users to optimize the sensitivity curve in a particular frequency region. Both techniques will be used on a larger scale in more advanced antennas.

[4] *http://tamago.mtk.nao.ac.jp*

[5] *http://www.gravity.uwa.edu.au/Stageone.html*

5.4 Existing Large Scale Antennas

Two large (kilometric) scale facilities have been built up to now. The American LIGO project[6] was planned at the beginning of the nineties after decades of intensive R&D efforts at MIT and CalTech under the leadership of Rainer Weiss, Kip Thorne and Ronald Drever and resulted in a consistent program headed by Rochus Vogt. The construction began in 1994 and was completed in 2002. The LIGO system is comprised of two sites, one at Hanford (WA) housing two antennas (4 km and 2 km) in the same set of vacuum pipes, and one at Livingston (LA) housing a single antenna (4 km). The two sites are about 3 000 km apart. The first science runs were performed in 2002. The target sensitivity has now been attained.

The Virgo antenna (France and Italy) was approved in 1994 and the construction began in 1996. The site is located at Cascina near Pisa (Italy) and the size of the antenna is 3 km (see Fig. 20). The first operation with the complete system took place in 2002. The first science runs are beginning. The target sensitivity has not yet been reached.

The American and French-Italian instruments are essentially the same, except for the different seismic isolation systems, which for Virgo is more elaborate (and more difficult to tune).

The result of a recent run of Virgo is shown in Figure 21.

Fig. 20 Aerial view of Virgo (see *http://wwwcascina.virgo.infn.it/Outreach/FotoSito/*).

6 LISA

LISA[7] is a joint ESA/NASA project scheduled for 2017, aiming to detect gravitational waves of very low frequency, from 0.1 mHz to 0.1 Hz. This frequency band is especially rich in exciting astrophysical events related to black holes. Monochromatic emissions from the population of galactic white dwarfs also fall in the same frequency range. The rate of events foreseen with a high signal to noise ratio is exceptionally high because this frequency range corresponds to the coalescence of massive black holes, emitting gravitational waves with an amplitude detectable over cosmological distances,

[6] *http://www.ligo.caltech.edu*

[7] *http://lisa.nasa.gov*

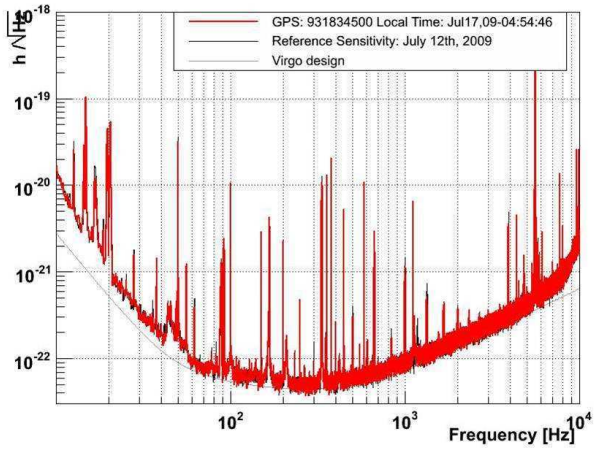

Fig. 21 Current spectral sensitivity of Virgo (courtesy of the Virgo collaboration).

thus involving a huge volume of the universe. The LISA system involves three spacecraft forming an equilateral triangle in a heliocentric orbit. One side of the triangle is 5 Mkm long. The spacecraft are linked by laser beams, and the gravitational signal is read on the relative Doppler shift of the incoming light compared to the local reference. The various technological challenges were addressed and reference solutions determined. The technology demonstrator "LISA Pathfinder" is currently scheduled to be launched in June 2011 in order to test its components and its proposed drag-free operation.

6.1 Orbits

Maintaining a stable triangular formation of spacecraft over several years is possible due to a property of central potentials. It is possible to position the three spacecraft in three weakly eccentric keplerian orbits, weakly inclined to the ecliptic plane with their major axes rotated by $2\pi/3$ relative to each other, in such a way that the plane defined by the triangle is inclined by 60 degrees from the ecliptic. The triangle is then static in a co-moving frame, at least to the first order in eccentricity. Namely, if we denote by L the nominal inter-spacecraft distance (~ 5 Mkm) and R the radius of the circular orbit (~ 150 Mkm), then the ratio $\alpha = L/2R$ is small ($\sim 1/60$), and the inclination angle relative to the ecliptic is chosen as

$$\epsilon = \arctan\left[\frac{\alpha}{1+\alpha/\sqrt{3}}\right], \tag{52}$$

(see Fig. 22).

The eccentricity is given by

$$e = \sqrt{1+\frac{2\alpha}{\sqrt{3}}+\frac{4\alpha^2}{3}} - 1. \tag{53}$$

This correlated choice of inclination and eccentricity is necessary for obtaining 60 degrees angles between the ecliptic and the plane defined by the constellation. This will be explained later. The three orbits are then defined by the following criteria:

– The three orbits are identical up to a rotation
– The semimajor axis of the second orbit is shifted 120 degrees with respect to the first one, and also the third with respect to the second, etc.
– The eccentric anomalies are shifted in the same order.

For spacecraft #1, one solves for the eccentric anomalies $E_i(t)$

$$E_i(t) - e\sin E_i(t) = \Omega t - (i-1)\frac{2\pi}{3}.$$

The ordinary Keplerian orbit is then (parameterized by time) of the form

$$\begin{cases} x_i''(t) = R(\cos E_i - e), \\ y_i''(t) = R\sqrt{1-e^2}\,\sin E_i, \\ z_i''(t) = 0. \end{cases} \tag{54}$$

Then new coordinates are found after a first rotation of angle ϵ of (54) in the (x'', z'') plane (see Fig. 22) giving

$$\begin{cases} x_i'(t) = R(\cos E_i - e)\cos\epsilon, \\ y_i'(t) = R\sqrt{1-e^2}\,\sin E_i, \\ z_i'(t) = -R(\cos E_i - e)\sin\epsilon. \end{cases} \tag{55}$$

Finally, a second rotation of angle $\theta_i = (i-1)\frac{2\pi}{3}$ in the (x', y') plane yields the actual coordinates

$$\begin{cases} x_i(t) = x_i'(t)\cos\theta_i - y_i'(t)\sin\theta_i, \\ y_i(t) = x_i'(t)\sin\theta_i + y_i'(t)\cos\theta_i, \\ z_i(t) = x_i'(t). \end{cases} \tag{56}$$

It is easy to see that at first order in e, the position of spacecraft number a is

$$\boldsymbol{x}_a(t) = \boldsymbol{r}_0(t) + 2eR\,\boldsymbol{u}_a(t),$$

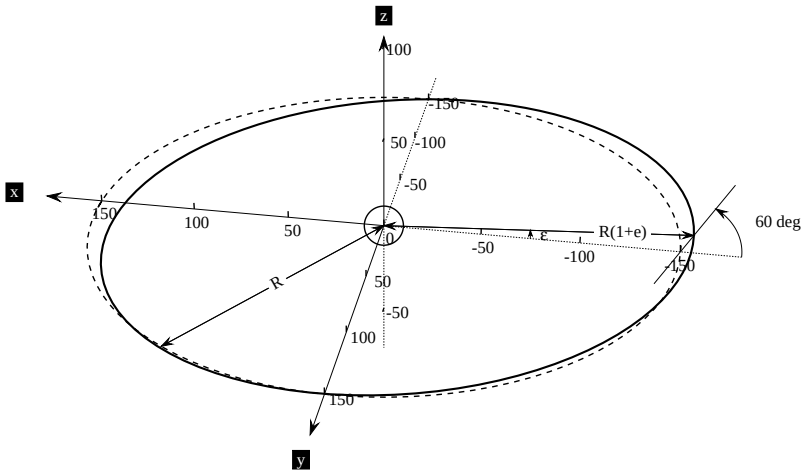

Fig. 22 *Dashed:* reference circular orbit. *Solid:* orbit of one spacecraft.

where $\boldsymbol{r}_0(t)$ is the motion of the center of mass along the orbit of radius R (1 AU)

$$\boldsymbol{r}_0(t) = \begin{pmatrix} R\cos\Phi \\ R\sin\Phi \\ 0 \end{pmatrix}$$

with $\Phi = \Phi(t) = 2\pi t/T$ ($T = 1$ yr). The $\boldsymbol{u}_a$ are unit vectors given by

$$\boldsymbol{u}_1(t) = \frac{1}{4}\begin{pmatrix} \cos 2\Phi - 3 \\ \sin 2\Phi \\ -2\sqrt{3}\cos\Phi \end{pmatrix}, \tag{57}$$

$$\boldsymbol{u}_2(t) = \frac{1}{4}\begin{pmatrix} \cos(2\Phi - 2\pi/3) + 3/2 \\ \sin(2\Phi - 2\pi/3) - 3\sqrt{3}/2 \\ -2\sqrt{3}\cos(\Phi - 2\pi/3) \end{pmatrix}, \tag{58}$$

$$\boldsymbol{u}_3(t) = \frac{1}{4}\begin{pmatrix} \cos(2\Phi - 4\pi/3) + 3/2 \\ \sin(2\Phi - 4\pi/3) + 3\sqrt{3}/2 \\ -2\sqrt{3}\cos(\Phi - 4\pi/3) \end{pmatrix}. \tag{59}$$

One can check that $\| \boldsymbol{u}_a(t) - \boldsymbol{u}_b(t) \| = \sqrt{3}$ $(a \neq b)$, so that the mutual distances of the spacecraft are indeed $2eR\sqrt{3} = L + \mathcal{O}(e^2 R)$ as desired. The unit vectors along the arms are

$$n_1(t) = \frac{\boldsymbol{u}_2 - \boldsymbol{u}_3}{\sqrt{3}},$$

(and circular permutations) given by

$$\boldsymbol{n}_1(t) = \frac{1}{4}\begin{pmatrix} \sin 2\Phi \\ -\cos 2\Phi - 3 \\ -2\sqrt{3}\sin\Phi \end{pmatrix}, \tag{60}$$

$$\boldsymbol{n}_2(t) = \frac{1}{4}\begin{pmatrix} \sin(2\Phi - 2\pi/3) + 3\sqrt{3}/2 \\ -\cos(2\Phi - 2\pi/3) + 3/2 \\ -2\sqrt{3}\sin(\Phi - 2\pi/3) \end{pmatrix}, \tag{61}$$

$$\boldsymbol{n}_3(t) = \frac{1}{4}\begin{pmatrix} \sin(2\Phi + 2\pi/3) - 3\sqrt{3}/2 \\ -\cos(2\Phi + 2\pi/3) + 3/2 \\ -2\sqrt{3}\sin(\Phi + 2\pi/3) \end{pmatrix}. \tag{62}$$

The orbital evolution of LISA over 1 yr is represented in Figure 23.

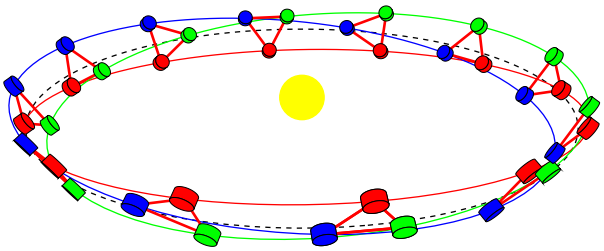

Fig. 23 Evolution of the LISA triangle over 1 yr.

6.2 Transfer Function

From Equation (6), it is possible to give the response of the six detectors to a gravitational wave

$$U_1 \;=\; -\,\frac{1}{2(1+\boldsymbol{w}\cdot\boldsymbol{n}_2)}\,[H_2(t-\mu_1)-H_2(t-\mu_3-L_2)]\,, \tag{63}$$

$$V_1 \;=\; \frac{1}{2(1-\boldsymbol{w}\cdot\boldsymbol{n}_3)}\,[H_3(t-\mu_1)-H_3(t-\mu_2-L_3)]\,, \tag{64}$$

and all others are obtained by circular permutations of indices. The notation is

$$\mu_a \;\equiv\; \boldsymbol{w}\cdot\boldsymbol{x}_a,$$

$$H_a(t) \;\equiv\; h_+(t)\,\xi_{+,a}+h_\times(t)\,\xi_{\times,a},$$

where $h_{+,\times}$ are the two polarization components of the gravitational wave. The directional functions $\xi_{+,\times,a}$ are defined by

$$\xi_{+,a}=(\boldsymbol{\theta}\cdot\boldsymbol{n}_a)^2-(\boldsymbol{\varphi}\cdot\boldsymbol{n}_a)^2,$$

$$\xi_{\times,a}=2(\boldsymbol{\theta}\cdot\boldsymbol{n}_a)(\boldsymbol{\varphi}\cdot\boldsymbol{n}_a)\,.$$

The unit vectors $\boldsymbol{\theta}$ and $\boldsymbol{\varphi}$ are related to the source direction

$$\boldsymbol{\theta}=\frac{\partial\boldsymbol{w}}{\partial\theta}=\begin{pmatrix}\cos\theta\,\cos\varphi\\ \cos\theta\,\sin\varphi\\ -\sin\theta\end{pmatrix},$$

$$\boldsymbol{\varphi}=\frac{1}{\sin\theta}\,\frac{\partial\boldsymbol{w}}{\partial\varphi}=\begin{pmatrix}-\sin\varphi\\ \cos\varphi\\ 0\end{pmatrix}.$$

Thus $U_1(t)$ is the signal produced on spacecraft #1 via the beam coming from spacecraft #3, whereas V_1 is the signal produced on spacecraft #1 via the beam coming from spacecraft #2.

6.3 Optical Links

The laser beams joining the spacecraft are passed through a magnifying telescope in order to generate a beam of width a, about 20 cm. If the receiving telescope has a comparable collecting area, the ratio of the power ΔP received after a trip of $L=5$ Mkm to the emitter power P is approximately given by

$$\frac{\delta P}{P}=\frac{\pi^2a^4}{\lambda^2L^2}\;\sim\;6\times10^{-10},$$

so that with a 1 W emitter, about 600 pW can be received after diffraction.

6.4 TDI

For the sake of simplicity, we consider only one laser per spacecraft (assuming, for instance, that the two lasers onboard are locked in phase). Fluctuations of the frequencies of the three lasers are obviously in competition with the gravitational wave signal. If we ignore the gravitational wave, the six data flows depend on the relative frequency excursions $C_i(t)\equiv\delta\nu_i(t)/\nu_0$ $(i=1,2,3)$, (ν_0 is the nominal common frequency). Here, we introduce possible departures of the arm lengths from their nominal value L due to the small residual periodic distortions or to errors in the positioning procedure. The armlengths are thus L_1 from spacecraft #3 to spacecraft #2 and so on by circular permutation.

Namely,

$$\begin{cases} U_1(t) = C_3(t - L_2) - C_1(t), \\ V_1(t) = C_1(t) - C_2(t - L_3), \end{cases} \tag{65}$$

(and circular permutations). It is worth introducing the delay operators D_i

$$(D_i * f)(t) \equiv f(t - L_i) \text{ for any function } f. \tag{66}$$

The data (65) become

$$\begin{cases} U_1 = D_2C_3 - C_1, \\ U_2 = D_3C_1 - C_2, \\ U_3 = D_1C_2 - C_3, \\ V_1 = C_1 - D_3C_2, \\ V_2 = C_2 - D_1C_3, \\ V_3 = C_3 - D_2C_1. \end{cases} \tag{67}$$

It is now easy to see that some combinations of data exist, giving identically zero in the case of pure laser noise. For instance, by forming the sums $U_a + V_a$, one obtains a kind of 3-vector having the algebraic signature of a curl

$$\boldsymbol{U} + \boldsymbol{V} = \boldsymbol{D} \times \boldsymbol{C}\,,$$

so that applying the divergence operator identically yields zero

$$\boldsymbol{D} \cdot (\boldsymbol{U} + \boldsymbol{V}) = 0.$$

In terms of the data flows, this is

$$\sum_{i=1}^{3} D_iU_i + \sum_{i=1}^{3} D_iV_i = 0.$$

This exhibits an example of a combination of delayed data which is insensitive to individual frequency fluctuations. We clearly have to look for all combinations having the same property. These combinations, as pointed out in Dhurandhar et al. (2002), have the form of a scalar product of a vector of formal polynomials in D_i with the data 6-tuple $U = (U_i, V_i)$. A generic combination X with delays is of the form

$$\sum_{i=1}^{3} (p_iV_i + q_iU_i) = \langle X|U\rangle,$$

where the 6-tuple $X = (p_i, q_i)$ contains the polynomials. The simplest case, as just shown, is

$$\zeta = (\boldsymbol{p}, \boldsymbol{q}) = (D_1, D_2, D_3, D_1, D_2, D_3).$$

The preceding combinations and other ones were first found by Tinto and colleagues (Armstrong et al. 1999). These are, besides ζ

$$\alpha = (1,\ D_3,\ D_1D_3,\ 1,\ D_1D_2,\ D_2),$$

with the two circular permutations (of the indices and of the places in the sub-3-tuple of the 6-tuple)

$$\beta = (D_1D_2,\ 1,\ D_1,\ D_3,\ 1,\ D_2D_3),$$

$$\gamma = (D_2,\ D_2D_3,\ 1,\ D_1D_3,\ D_1,\ 1).$$

It is worth noting that in a circular permutation of the indices and of the places in the sub-3-tuples:

$$\alpha \to \beta \to \gamma \to \alpha, \tag{68}$$

whereas

$$\zeta \to \zeta. \tag{69}$$

The set $\mathcal{P}_3$ of all polynomials in three variables (D_1, D_2, D_3) has the algebraical structure of a ring.

It can be shown (Dhurandhar et al. 2002) that the set of all noise cancelling combinations has the structure of a module on the polynomial ring, and that $\alpha, \beta, \gamma, \zeta$ build a complete set of generators of the module. In other words, any noise canceling combination is a combination of $\alpha, \beta, \gamma, \zeta$. For instance, Tinto & Armstrong (1999) proposed the "Michelson" combinations

$$X_1 = \alpha - D_3\beta - D_2\gamma + D_2D_3\zeta.$$

X_2 and X_3 are obtained by circular permutations of the indices and of the generators, according to Equations (68) and (69).

6.5 Spectral Sensitivity

6.5.1 Noise power spectral density

The realistic situation is slightly more complicated because there are actually six lasers, the optical benches are not fixed with respect to the reference mass, and the reference mass itself has a small but finite residual motion due to the capacitive readout system. In the optical detection process, the weakness of the light power coming from far away induces a non-negligible shot noise. The noisy part of the data flows must therefore be completed. We denote by a * the part of a spacecraft facing another spacecraft in the direct sense (see Fig. 24). We denote by $\boldsymbol{V}_i$, $\boldsymbol{V}_i^*$ the velocities of the optical benches, and by $\boldsymbol{v}_i$, $\boldsymbol{v}_i^*$ the velocities of the reference masses. The apparent frequency jitter due to shot noise is denoted by y_i, y_i^*.

The differential frequency recorded at spacecraft #1 with respect to the light coming from spacecraft #3, therefore, has several components (we follow Tinto et al. 2004):

– A Doppler shift due to the motion of the far optical bench for which we take the retarded value

$$-\boldsymbol{n}_2 \cdot \boldsymbol{V}_3(t - L_2).$$

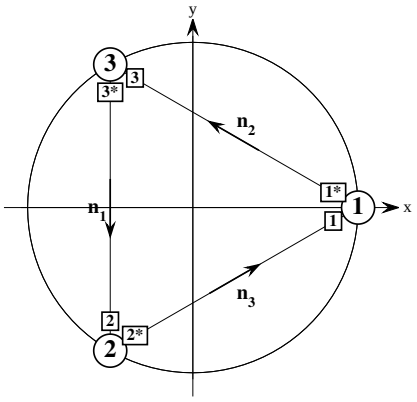

Fig. 24 Notation for the data flows.

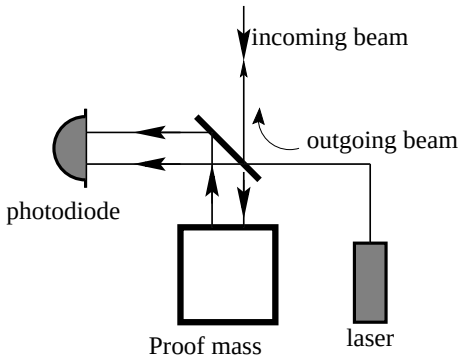

Fig. 25 Inter spacecraft exchanges.

– A Doppler shift due to the motion of the local optical bench

$$\boldsymbol{n}_2 \cdot \boldsymbol{V}_1^*(t).$$

– A Doppler shift due to the fact that the incoming beam is reflected on the test mass before mixing with the local laser light (hence the factor of 2)

$$2\boldsymbol{n}_2 \cdot \boldsymbol{v}_1^*(t),$$

(see Fig. 25), so that the data U_1 must be generalized as follows:

$$U_1(t) = C_3(t - L_2) - C_1^*(t) - \boldsymbol{n}_2 \cdot \boldsymbol{V}_3(t - L_2) - \boldsymbol{n}_2 \cdot \boldsymbol{V}_1^*(t) + 2\boldsymbol{n}_2 \cdot \boldsymbol{v}_1^*(t) + y_1^* \,. \tag{70}$$

In the same way, we have

$$V_1(t) = C_1(t) - C_2^*(t - L_3) - \boldsymbol{n}_3 \cdot \boldsymbol{V}_2^*(t - L_3) - \boldsymbol{n}_3 \cdot \boldsymbol{V}_1(t) + 2\boldsymbol{n}_3 \cdot \boldsymbol{v}_1(t) + y_1. \tag{71}$$

We must also take into account the noises induced by the internal frequency monitoring aboard spacecraft #1. A part of the laser #1 light is bounced on the test mass before being sent to part #1* through an optical fiber (see Fig. 26). The received beam undergoes no Doppler shift because it is transmitted through the extraction optics of the fiber which is linked to the optical bench. The emitted beam gets a first Doppler shift due to motion of the laser and a second one due to the motion of the injection optics of the fiber (both linked to the optical bench) (whence a factor of 2). There is also a Doppler shift due to reflection on the test mass before being sent. The result of the frequency monitoring in the "left" part of spacecraft #1 is therefore

$$z_1(t) = C_1(t) - C_1^*(t) + 2\boldsymbol{n}_2 \cdot (\boldsymbol{v}_1^*(t) - \boldsymbol{V}_1^*(t)) + \sigma_1. \tag{72}$$

While in the "right" part, the monitoring gives

$$z_1^*(t) = C_1^*(t) - C_1(t) - 2\boldsymbol{n}_3 \cdot (\boldsymbol{v}_1(t) - \boldsymbol{V}_1(t)) + \sigma_1. \tag{73}$$

In the preceding formulas, we have ignored time delays and the shot noise. We have however introduced an extra source of noise due to vibrations of the transmitting fiber (assumed reciprocal) and denoted it by σ_1. Data flows onboard spacecraft #2 and #3 are obtained from (70, 71, 72, 73) by

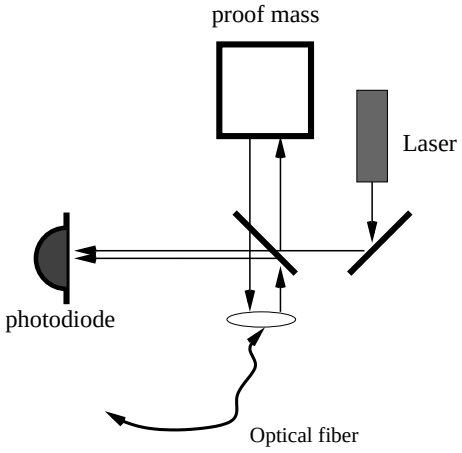

Fig. 26 Internal exchanges.

circularly permuting the indices. In the preceding paragraph, we have found combinations able to cancel the laser frequency noise (the C_i). In fact, the same combinations can suppress the noise coming from the random motions of the optical benches (this is intuitively obvious for it is impossible to distinguish between the two effects in the emitted light). If we forget the proof masses' motions, we can write

$$U_1 = D_2(C_3 - \boldsymbol{n}_2 \cdot \boldsymbol{V}_3) - (C_1^* + \boldsymbol{n}_2 \cdot \boldsymbol{V}_1^*),$$
$$V_1 = (C_1 - \boldsymbol{n}_3 \cdot \boldsymbol{V}_1) - D_3(C_2^* + \boldsymbol{n}_3 \cdot \boldsymbol{V}_2^*),$$

and we can form a new data set

$$Z_1 = \frac{z_1 - z_1^*}{2}.$$

If we define new variables as

$$\tilde{C}_1 = C_1 - \boldsymbol{n}_3 \cdot \boldsymbol{V}_1, \;\; \tilde{C}_1^* = C_1^* + \boldsymbol{n}_2 \cdot \boldsymbol{V}_1^*,$$

the preceding equations simply become

$$\begin{aligned} U_1 &= D_2\tilde{C}_3 - \tilde{C}_1^*, \\ V_1 &= \tilde{C}_1 - D_3\tilde{C}_2^*, \\ Z_1 &= \tilde{C}_1 - \tilde{C}_1^*, \end{aligned}$$

so that the algebraic structure is identical to the simple situation of the preceding paragraph. There therefore exists a module of noise canceling combinations that is an extension of the preceding discussion. The data flow is now a set of 9-tuples $U = (U_i, V_i, Z_i)$, and the module of "silent" combinations is generated by the following 9-tuples

$$\alpha = (1, D_3, D_1D_3, 1, D_1D_2, D_2, -1 - D_1D_2D_3, -(D_1D_2 + D_3), -(D_1D_3 + D_2)). \quad (74)$$
$$\beta = (D_1D_2, 1, D_1, D_3, 1, D_2D_3, -(D_1D_2 + D_3), -1 - D_1D_2D_3, -(D_2D_3 + D_1)). \quad (75)$$
$$\gamma = (D_2, D_2D_3, 1, D_1D_3, D_1, 1, -(D_1D_3 + D_2), -(D_2D_3 + D_1), -1 - D_1D_2D_3). \quad (76)$$
$$\zeta = (D_1, D_2, D_3, D_1, D_2, D_3, -(D_1 + D_2D_3), -(D_2 + D_3D_1), -(D_3 + D_1D_2)). \quad (77)$$

If we denote by (p_i, q_i, r_i) the components of a generic generator g, a silent combination will be denoted by

$$\langle g|U\rangle = \sum_{i=1}^{3} \left[p_iV_i + q_iU_i + r_iZ_i\right].$$

Once the spurious effects of the lasers and optical benches are canceled, we are left with the residual noise coming from the spurious motions of the proof masses, and from shot noise. Since these two kinds of noises are purely local, there is no hope of canceling them by any combination. The preprocessed data are thus of the form (we ignore possible gravitational signals)

$$\begin{aligned} U_1 &= 2\boldsymbol{n}_2 \cdot \boldsymbol{v}_1^* + y_1^*, \\ V_1 &= 2\boldsymbol{n}_3 \cdot \boldsymbol{v}_1 + y_1, \\ Z_1 &= \boldsymbol{n}_3 \cdot \boldsymbol{v}_1 + \boldsymbol{n}_2 \cdot \boldsymbol{v}_1^*. \end{aligned}$$

If we consider the part coming from the proof masses (acceleration noise), a generic combination gives

$$\langle g|U\rangle_{\rm acc} = (2p_1 + r_1)\boldsymbol{v}_1 \cdot \boldsymbol{n}_3 + (2p_2 + r_2)\boldsymbol{v}_2 \cdot \boldsymbol{n}_1 + (2p_3 + r_3)\boldsymbol{v}_3 \cdot \boldsymbol{n}_2 +$$
$$+(2p_1 + r_1)\boldsymbol{v}_1^* \cdot \boldsymbol{n}_2 + (2p_2 + r_2)\boldsymbol{v}_2^* \cdot \boldsymbol{n}_3 + (2p_3 + r_3)\boldsymbol{v}_3^* \cdot \boldsymbol{n}_1.$$

In the same way, we find for the shot noise contribution

$$\langle g|U\rangle_{\rm sn} = \sum (q_i y_i^* + p_i y_i).$$

After a Fourier transform, the delay operators reduce to phase factors

$$D_i \ \rightarrow \ {\rm e}^{i\omega L_i}.$$

We shall treat the $\boldsymbol{v}_i \cdot \boldsymbol{n}_j$ and $\boldsymbol{v}_i^* \cdot \boldsymbol{n}_j$ as

- uncorrelated,
- having identical PSDs.

and the same for the y_i and y_i^*. We denote by $S_{\rm acc}(f)$ the PSD common to all $\boldsymbol{v}_i \cdot \boldsymbol{n}_j$ and $\boldsymbol{v}_i^* \cdot \boldsymbol{n}_j$ (acceleration noise), and $S_{\rm sn}$ is the PSD of the y_i , y_i^* (shot noise for brevity). Then the global noise PSD is of the form

$$S_g(f) = \sum_{i=1}^{3} \left\{ |2p_i + r_i|^2 \ + \ |2q_i + r_i|^2 \right\} \, S_{\rm acc}(f) + \sum_{i=1}^{3} \left\{ |p_i|^2 + |q_i|^2 \right\} \, S_{\rm bq}(f). \qquad (78)$$

To be specific, we detail the computation of the noise PSD of the α generator. In the TDI pre-processed data, we may assume a regular triangle ($L_1 = L_2 = L_3 = L$) and we have (the arrows denote a Fourier transform)

$$\begin{array}{ll}
2p_1 + r_1 = 2 - 1 - D_1 D_2 D_3 & \rightarrow \ 1 - {\rm e}^{3i\omega L}, \\
2p_2 + r_2 = 2D_3 - D_1 D_2 - D_3 & \rightarrow \ {\rm e}^{i\omega L} - {\rm e}^{2i\omega L}, \\
2p_3 + r_3 = 2D_1 D_3 - D_1 D_3 - D_2 & \rightarrow \ {\rm e}^{2i\omega L} - {\rm e}^{i\omega L}, \\
2q_1 + r_1 = 2 - 1 - D_1 D_2 D_3 & \rightarrow \ 1 - {\rm e}^{3i\omega L}, \\
2q_2 + r_2 = 2D_1 D_2 - D_1 D_2 - D_3 & \rightarrow \ {\rm e}^{2i\omega L} - {\rm e}^{i\omega L}, \\
2q_3 + r_3 = 2D_2 - D_1 D_3 - D_2 & \rightarrow \ {\rm e}^{i\omega L} - {\rm e}^{2i\omega L},
\end{array}$$

so that we have

$$S_{\alpha,{\rm acc}}(f) = \left[8 \sin^2(3\pi f L) + 16 \sin^2(\pi f L) \right] S_{\rm acc}(f),$$

and because the p_i, q_i of α are simple phase factors,

$$S_{\alpha,{\rm sn}}(f) = 6 \, S_{\rm sn}(f),$$

so that the total PSD is

$$S_\alpha(f) = \left[8 \sin^2(3\pi f L) + 16 \sin^2(\pi f L) \right] S_{\rm acc}(f) + 6 \, S_{\rm sn}(f).$$

It is currently assumed (Tinto et al. 2004) that the PSDs $S_{\rm acc}(f)$ and $S_{\rm bq}(f)$ obey the very simple following models:

$$S_{\rm acc}(f) = s_1 \left[\frac{1{\rm Hz}}{f} \right]^2, \qquad (79)$$

with

$$s_1 = 2.5 \ \times \ 10^{-48} \ {\rm Hz}^{-1},$$

and

$$S_{\rm bq}(f) = s_2 \left[\frac{f}{1{\rm Hz}} \right]^2, \qquad (80)$$

with

$$s_2 = 1.8 \ \times \ 10^{-37} \ {\rm Hz}^{-1}.$$

6.5.2 GW signal in Fourier space

It is easy to find the transfer functions for GW signals. For instance, we get from (63)

$$F_{U_1,+,\times} = i\,\pi f L\,\mathrm{e}^{i\omega(L-\mu_2)/2}\,\mathrm{sinc}[\pi f L(1+\boldsymbol{w}\cdot\boldsymbol{n}_2)]\;\xi_{2,+,\times}, \tag{81}$$

$$F_{U_2,+,\times} = i\,\pi f L\,\mathrm{e}^{i\omega(L-\mu_3)/2}\,\mathrm{sinc}[\pi f L(1+\boldsymbol{w}\cdot\boldsymbol{n}_3)]\;\xi_{3,+,\times}, \tag{82}$$

$$F_{U_3,+,\times} = i\,\pi f L\,\mathrm{e}^{i\omega(L-\mu_1)/2}\,\mathrm{sinc}[\pi f L(1+\boldsymbol{w}\cdot\boldsymbol{n}_1)]\;\xi_{1,+,\times}. \tag{83}$$

In the same way, we have

$$F_{V_1,+,\times} = -\,i\,\pi f L\,\mathrm{e}^{i\pi f(L-\mu_3)}\,\mathrm{sinc}[\pi f L(1-\boldsymbol{w}\cdot\boldsymbol{n}_3)]\xi_{3,+,\times}, \tag{84}$$

$$F_{V_2,+,\times} = -\,i\,\pi f L\,\mathrm{e}^{i\pi f(L-\mu_1)/2}\,\mathrm{sinc}[\pi f L(1-\boldsymbol{w}\cdot\boldsymbol{n}_1)]\;\xi_{1,+,\times}, \tag{85}$$

$$F_{V_3,+,\times} = -\,i\,\pi f L\,\mathrm{e}^{i\pi f(L-\mu_2)/2}\,\mathrm{sinc}[\pi f L(1-\boldsymbol{w}\cdot\boldsymbol{n}_2)]\;\xi_{2,+,\times}. \tag{86}$$

The transfer function for a generic combination $g=(p_i,q_i,r_i)$ is now

$$F_{X,+,\times} = \langle X|\boldsymbol{F}\rangle = \sum_{i=1}^{3}\left(\tilde{p}_i\,F_{V_i,+,\times}\;+\tilde{q}_i\,F_{U_i,+,\times}\right), \tag{87}$$

where the $\tilde{p}_i$, $\tilde{q}_i$ are true polynomials of the unique variable $\exp(2i\pi fL)$. If we consider a gravitational signal, the corresponding data generated by g in the Fourier domain is

$$g(f) = (\boldsymbol{p}\cdot\boldsymbol{F}_{V,+}+\boldsymbol{q}\cdot\boldsymbol{F}_{U,+})\tilde{h}_+ + (\boldsymbol{p}\cdot\boldsymbol{F}_{V,\times}+\boldsymbol{q}\cdot\boldsymbol{F}_{U,\times})\tilde{h}_\times\,.$$

In order to get a spectral density, we consider the functions $h_+(t)$ and $h_\times(t)$ to be stochastic processes, and we take the expectation value of the square modulus

$$S_{g,\mathrm{signal}}(f) = \langle\,|g(f)\,|^2\rangle.$$

If we take an average of the polarization angles, the crossed terms $h_+.h_\times$ disappear from the preceding expression. We may furthermore take the same spectral density S_h for h_+ and $h_\times$, so that the averaged spectral density of the signal is

$$\langle S_{g,\mathrm{signal}}(f)\rangle = \left[\sum_{i=1}^{3}|p_iF_{V_i,+}+q_iF_{VU_i,+}|^2+\sum_{i=1}^{3}|p_iF_{V_i,\times}+q_iF_{VU_i,\times}|^2\right]S_h(f).$$

6.5.3 Signal to noise ratio

The square of the signal to noise ratio of the g combination is

$$\mathrm{RSB}_g(f)^2 = \rho_g(f)\,S_h(f),$$

with

$$\rho(f) = \frac{\sum_{i=1}^{3}|p_iF_{V_i,+}+q_iF_{VU_i,+}|^2+\sum_{i=1}^{3}|p_iF_{V_i,\times}+q_iF_{VU_i,\times}|^2}{S_g(f)}.$$

In order to give a synthetic estimation, it is usual to first take an average over the direction of the source (θ,ϕ)

$$\langle\rho_g(f)\rangle = \frac{1}{4\pi}\int_0^{2\pi}d\phi\int_0^{\pi}\sin\theta\,d\theta\,\rho_g(\theta,\phi,f).$$

It is difficult to analytically treat this average, but the numerical integration is straightforward. Secondly, we assume an integration time of $T=1\,\mathrm{yr}$ and a signal to noise ratio of 5, which gives the averaged spectral sensitivity

$$h_g(f) = \frac{5}{\sqrt{\langle\rho_g(f)\rangle\,T}}. \tag{88}$$

Figure 27 shows the spectral sensitivity of the "Michelson interferometer" under these conventions.

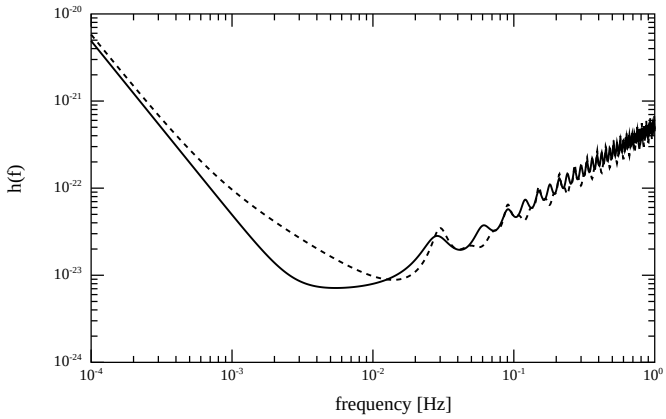

Fig. 27 Spectral sensitivity of two TDI combinations. "Michelson interferometer" (*solid curve*) and α (*dashed curve*).

7 CONCLUSIONS AND PERSPECTIVES

Actual terrestrial instruments have began to operate in practically nominal conditions. We know that improvements are necessary for reaching a sensitivity level that allows astrophysical studies. These improvements require efforts on all the subsystems we have discussed above. For instance, fiber lasers offer an interesting solution for increasing the primary power up to hundreds of watts, and decreasing the shot noise by possibly one order of magnitude. Thermal problems could be fixed by changing the modal structure of the laser beam or by active thermal compensation systems. Thermal noise in the suspensions of mirrors is reduced by using monolithic systems. An R&D research program is funded in the U.S.A. around "Advanced LIGO," and similarly some improvements are being planned for an "Advanced Virgo." A large program for a cryogenic 3km interferometer is planned in Japan[8].

The recent recommendation by the National Research Council of the United States (Astro2010 review) of LISA as the second major mission in Astronomy and Astrophysics will trigger new proposals for the technology, and a large international effort for organizing the LISA Data Analysis community at the end of the present decade.

References

Abbott, B., Abbott, R., Adhikari, R., et al. 2004, Nuclear Instruments and Methods in Physics Research A, 517, 154

Armstrong, J. W., Estabrook, F. B., & Tinto, M. 1999, ApJ, 527, 814

Astone, P., Ballantini, R., Babusci, D., et al. 2008, Classical and Quantum Gravity, 25, 114048

Astone, P., Ballantini, R., Babusci, D., et al. 2006, Classical and Quantum Gravity, 23, 57

Astone, P., Bassan, M., Bonifazi, P., et al. 1993, Phys. Rev. D, 47, 362

Baggio, L., Bignotto, M., Bonaldi, M., et al. 2005, Phys. Rev. Lett., 95, 081103

Blanchet, L., Faye, G., & Nissanke, S. 2005, Phys. Rev. D, 72, 044024

Bonazzola, S., & Marck, J. A. 1993, A&A, 267, 623

Bondu, F., Hello, P., & Vinet, J. 1998, Phys. Lett. A, 246, 227

[8] *http://gw.icrr.u-tokyo.ac.jp/lcgt*

Brillet, A., Vinet, J., Loriette, V., et al. 2003, Phys. Rev. D, 67, 102006
Buonanno, A., & Damour, T. 2000, Phys. Rev. D, 62, 064015
Callen, H. B., & Welton, T. A. 1951, Phys. Rev., 83, 34
Chandrasekhar, S. 1970, Phys. Rev. Lett., 24, 611
de Waard, A., Benzaim, Y., Frossati, G., et al. 2005, Classical and Quantum Gravity, 22, 215
Dhurandhar, S. V., Nayak, K. R., & Vinet, J. 2002, Phys. Rev. D, 65, 102002
Drever, R. W. P. 1983, in Lecture Notes in Physics, Berlin Springer Verlag, Vol. 124, Lecture Notes in Physics, Berlin Springer Verlag, 321
Forward, R. L. 1978, Phys. Rev. D, 17, 379
Gair, J. R., & Jones, G. 2006, ArXiv General Relativity and Quantum Cosmology e-prints
Gottardi, L. 2007, Phys. Rev. D, 75, 022002
Hughes, S. A. 2001, Classical and Quantum Gravity, 18, 4067
Levin, Y. 1998, Phys. Rev. D, 57, 659
Mauceli, E., Geng, Z. K., Hamilton, W. O., et al. 1996, Phys. Rev. D, 54, 1264
Meers, B. J. 1988, Phys. Rev. D, 38, 2317
Mours, B., Tournefier, E., & Vinet, J. 2006, Classical and Quantum Gravity, 23, 5777
Schnier, D., Mizuno, J., Heinzel, G., et al. 1997, Phys. Lett. A, 225, 210
Thorne, K. S. 1987,Gravitational radiation., eds. Hawking, S. W., & Israel, W. 330
Tinto, M., & Armstrong, J. W. 1999, Phys. Rev. D, 59, 102003
Tinto, M., Estabrook, F. B., & Armstrong, J. W. 2004, Phys. Rev. D, 69, 082001
Tourrenc, P. 1997, Relativity and Gravitation, ed. Tourrenc, P.
Vinet, J. 1979, Ann. Inst. Henri Poincaré, 3, 251
Vinet, J. 2009, Living Reviews in Relativity, 12, 5
Vinet, J., Meers, B., Man, C. N., & Brillet, A. 1988, Phys. Rev. D, 38, 433
Weber, J. 1960, Phys. Rev., 117, 306
Weiss, R. 1972, Quart. Progr. Rep. Lab. Electro. MIT, 105, 54
Zwerger, T., & Mueller, E. 1997, A&A, 320, 209